NUMERICAL ANALYSIS AND DESIGN OF SLENDER ELLIPTICAL HOLLOW SECTIONS IN BENDING

Finian McCann[a] and Leroy Gardner[b]

[a] School of the Built Environment and Architecture, London South Bank University, UK.
email: mccannf@lsbu.ac.uk.

[b] Department of Civil and Environmental Engineering, Imperial College London, UK.
email: leroy.gardner@imperial.ac.uk.

Keywords: Steel structural design; Elliptical hollow sections; Slender sections; Local buckling; Numerical modelling; Postbuckling.

Abstract. *The local buckling behaviour and ultimate cross-sectional resistance of slender tubular elliptical profiles in bending are examined by means of numerical modelling. After successful validation of the numerical model against previous experimental results, a parametric study comprising 240 simulations was conducted in order to investigate the influence of cross-section aspect ratio, axis of bending, geometric imperfections and local slenderness on structural behaviour. The ultimate moments, moment–curvature relationships and failure modes obtained are discussed. It was found that, overall, postbuckling stability increases and imperfection sensitivity decreases with increasing elliptical hollow section (EHS) aspect ratio. A design method is proposed for Class 4 EHS members that reflects the reduction in resistance due to local buckling with increasing slenderness and extends the range of applicability of existing provisions. A reliability analysis was performed in accordance with EN 1990, indicating that the design methods for EHS in bending, in addition to previous design methods for EHS in compression, are suitable for use in the Eurocode framework with a recommended partial factor of unity.*

1 INTRODUCTION

In recent years, structural steel elliptical hollow sections (EHS) have attracted increased research focus. This can be attributed to their introduction and availability as hot-finished products [1], their aesthetic properties, which have led to their use in high-profile projects such as Heathrow Terminal 5, Barajas Airport, Madrid, the University of Warwick and Cork Airport [2], and their enhanced flexural properties about the major principal axis when compared to circular hollow section (CHS) tubes [3]. Research into the structural response of EHS tubes has included testing, numerical modelling and the development of design rules for cross-

sections in compression and bending [4–7], analysis of the global buckling response of EHS columns [7,8], stainless steel EHS columns [9], EHS columns in fire [10], concrete-filled EHS columns [11–14], beams [15] and beam-columns [16], the behaviour of members in shear [17] and the postbuckling behaviour and strength of slender EHS tubes in compression [18].

The focus of the present study is the behaviour and resistance of slender EHS tubes in bending. Potential applications of such members include aesthetic lightweight cladding rails, mullion posts, thin-walled storage silos and concrete-filled steel tubes in composite construction [2,18]. A number of the current range of hot-finished elliptical hollow sections [19], which have been used in a variety of structural applications, as outlined in [2], are Class 4 in bending according to the limits proposed in [6] and the provisions of the upcoming revision to EN 1993-1-1 [20]. Although cold-formed profiles are not specifically addressed in the present study, it is envisaged that the findings and proposed design guidance also apply to these sections since the level of local geometric imperfections in cold-formed and hot-finished tubular sections are generally similar [21] and the dominant through-thickness residual stresses in cold-formed tubular sections have been shown not to have a strong influence on their local stability [22–23].

The elliptical hollow sections examined in the present study have a maximum outer radius a and a minimum outer radius b, and are assumed to be thin-walled with a constant wall thickness t, as shown in Figure 1; the major (y-y) and minor (z-z) cross-sectional axes are also indicated in Figure 1. Slender EHS, i.e., those that fail by local buckling prior to the attainment of their elastic moment resistance M_{el}, are the focus of the present study. The elastic moment resistance $M_{el} = W_{el} f_y$ is the product of the elastic section modulus W_{el} for the axis of bending being considered and the material yield strength f_y. The elastic section moduli for bending about either the major axis or the minor axis can be determined via integration around the circumference of the median profile [6], yielding Eq.(1) and Eq.(2) for the major axis elastic section modulus $W_{el,y}$ and the minor axis elastic section modulus $W_{el,z}$, respectively:

$$W_{el,y} = \frac{4a_m^3 t}{a} \int_0^{\pi/2} \cos^2\phi \sqrt{\sin^2\phi + \frac{b_m^2}{a_m^2}\cos^2\phi}\, d\phi \quad (1)$$

$$W_{el,z} = \frac{4a_m b_m^2 t}{b} \int_0^{\pi/2} \sin^2\phi \sqrt{\sin^2\phi + \frac{b_m^2}{a_m^2}\cos^2\phi}\, d\phi \quad (2)$$

where $a_m = (2a - t)/2$, $b_m = (2b - t)/2$ and ϕ is defined in Figure 1.

It has been found previously [18] that the postbuckling behaviour of slender EHS tubes in compression transitions from that of imperfection-sensitive cylindrical shells (unstable

postbuckling) for EHS with low cross-sectional aspect ratios a/b to that of imperfection-insensitive plates (stable postbuckling) for EHS with higher aspect ratios, in agreement with earlier analytical and numerical studies [24–27]. Thus, the postbuckling behaviour is a function of both cross-sectional aspect ratio and local slenderness (defined in Section 2.1.1), with the following observed trends being reflected in a design proposal [18] formulated on the basis of an associated parametric study: i) increasing stability of the postbuckling response, and thus greater normalised load–carrying capacity, with increasing aspect ratio; ii) increasing stability of the postbuckling response with increasing local slenderness; iii) decreasing imperfection sensitivity with increasing slenderness.

The present study aims to ascertain whether analogous relationships exist for EHS in bending. The development and validation of a numerical model to simulate the response of EHS tubes in bending is described. After achieving satisfactory agreement between the numerical results and previous experimental results [6], the response of EHS tubes with cross-sectional aspect ratios a/b ranging from 1.5 to 5.0, bent about either the major or minor axis, is examined. Other parameters varied in the study include the yield strength f_y, the tube wall thickness t (shown in Figure 1) and the imperfection amplitude Δw. The results of the parametric study are used as a basis for the formulation of resistance functions for the design of Class 4 (slender) EHS members in bending that extend the range of applicability of a design method included in the upcoming revision to EN 1993-1-1 [20]. A reliability analysis is performed in accordance with EN 1990 [28] in order to determine the minimum required partial factor to be used when applying the design methods; a reliability analysis is also performed on a design method for slender EHS in compression that is included in the upcoming revision to EN 1993-1-1 [20]. The objectives of the present study are thus: i) to establish a database of resistances of slender steel elliptical cross-sections in bending; ii) to assess the influences of various design parameters on these resistances, iii) to propose a design method for Class 4 EHS in bending and iv) to assess the suitability of design methods for slender EHS in either bending or compression for use within the Eurocode framework by determining minimum required partial factors.

2 DEVELOPMENT OF THE NUMERICAL MODEL

In this section, the approach employed to model the EHS tubes in bending using the finite element modelling software Abaqus [29] is described, followed by the validation of the model against previous experimental results [6]. The cross-sectional geometries, material properties

and modelling approach used in the numerical simulations are in line with those employed in [18].

2.1 Description of the numerical model

The modelling strategy employed in the present study is described in this sub-section, including the analysis procedure, meshing, the definition of imperfections and the material models used.

2.1.1 Slender EHS geometries

When considering circular hollow sections (CHS), the definition of Class 4 (slender) cross-sections in EN 1993-1-1 [20] is dependent on the diameter-to-thickness ratio D/t. For elliptical sections, the circular diameter D is replaced by an equivalent diameter D_{eq}, following the recommendations of [6], whereby:

For EHS in major axis bending:

$$D_{eq} = 2(b^2 / a) \quad \text{for } a/b \leq 1.357, \tag{3}$$

$$D_{eq} = 0.8(a^2 / b) \quad \text{for } a/b > 1.357, \tag{4}$$

For EHS in minor axis bending:

$$D_{eq} = 2(a^2 / b) \quad \text{for all aspect ratios.} \tag{5}$$

These definitions of D_{eq} relate to analytical predictions [30,31] of the location of the point of initiation of local buckling around the tube wall. For EHS in pure compression or bent about the minor axis, this critical point is located at the extreme of the minor axis (where the radius of curvature is at a maximum), while for EHS bent about the major axis, the critical point is located either at the extreme of the major axis or at an intermediate position, depending on the aspect ratio (see Figure 2). It has been proposed [6] that the condition for slender (Class 4) tubular sections bent about either the major axis or minor axis, adapted for use with EHS, can be taken as:

$$\frac{D_{eq}}{t\varepsilon^2} > 140 \tag{6}$$

where $\varepsilon = (235/f_y)^{0.5}$; this limit is to be incorporated in the upcoming revision of EN 1993-1-1 [20]. The corresponding limit for EHS in compression is $D_{eq}/t\varepsilon^2 = 90$.

Related to this measure of cross-sectional slenderness ($D_{eq}/t\varepsilon^2$) is the nondimensionalised local buckling slenderness $\bar{\lambda}_\ell$, which is defined in Eq.(7):

$$\bar{\lambda}_\ell = \sqrt{\frac{f_y}{f_{cr}}} \tag{7}$$

where f_{cr} is the elastic critical local buckling stress, adapted from the equivalent expression for CHS:

$$f_{cr} = \frac{E}{\sqrt{3(1-\nu^2)}}\frac{2t}{D_{eq}} \tag{8}$$

By setting $D_{eq}/t\varepsilon^2 = 140$ and taking $E = 216640$ N/mm^2, which represents an average value obtained from tensile coupon testing [5,6] and is used in the present numerical models, the value of $\bar{\lambda}_\ell$ corresponding to the Class 4 limit is found to be 0.355; for $E = 210000$ N/mm^2, the limit is $\bar{\lambda}_\ell = 0.360$.

Values of $D_{eq}/t\varepsilon^2$ for commercially-available hot-finished EHS [1] in grade S355 steel, which all have aspect ratios $a/b = 2.0$, range between about 50 and 150. Although high-strength steel (HSS) EHS are not yet commercially-available, given the recent developments for other HSS tubular sections [32,33], it can be assumed that EHS with values of f_y potentially as high as 960 N/mm^2 will be available in the near future. Considering these high strength steels, values of $D_{eq}/t\varepsilon^2$ increase to between about 130 and 400. When considering more slender sections becoming available, the cases considered in the present work encompass a comprehensive range of EHS that might be encountered in practice.

2.1.2 Meshing and boundary conditions

The EHS tubes were modelled in Abaqus [29] using 4-noded isoparametric reduced-integration S4R shell elements with a characteristic element size of 10 mm; it has been shown previously [18,27] that models using this mesh density can simulate the behaviour of thin-walled EHS tubes accurately [18,27].

Rigid plates were attached to the end sections of the tubes using tie constraints. These rigid end plates were modelled using either 3-noded R3D3 or 4-noded R3D4 finite elements; given

that the mesh seed density along the boundary of the plate was fixed, the selection of finite elements within the rigid plate had no influence on the overall behaviour of the EHS specimen. Fully-fixed boundary conditions were imposed on one end plate, while a concentrated moment was applied at the centroid of the end plate at the opposite end, which was orientated to simulate bending about either the major or minor cross-sectional axis as necessary. Rotation about the other cross-sectional axis was restrained, as were translation out of the plane of bending and rotation about the longitudinal axis of the tube.

2.1.3 Analysis procedure

The simulations comprised two steps. The first step was a linear eigenvalue analysis from which the elastic buckling stress for each buckling mode was obtained, with the critical buckling moment M_{cr} being that associated with the first valid buckling mode (see Section 2.1.5). The mode shape provided the form of the initial imperfection for the second step, a Riks arclength continuation analysis, which simulated the nonlinear behaviour of the EHS up to and beyond the ultimate moment.

2.1.4 Material modelling

For the linear eigenvalue analyses, the tube material was assumed to be homogeneous, isotropic and linearly-elastic with a Young's modulus of 216640 MPa and a Poisson's ratio of 0.3. For the Riks analyses, elastic–perfectly plastic material models were applied, with three different yield stresses considered for each aspect ratio (see Section 3.1). No residual stresses were included in the numerical analyses since they have been found to be of very low magnitude in hot-finished elliptical tubes [5,6].

2.1.5 Geometric imperfections

The initial imperfection mode shapes were based on previous guidance [27] whereby the mode shape was assumed to have an odd number of longitudinal half-waves along the tube length. In the interests of consistency, the same mode shapes were applied to sections with the same aspect ratio and length, which were extracted from linear eigenvalue analysis using wall thicknesses of 4.2 mm and 8.7 mm for tubes bent about their major and minor axes, respectively; EHS with thicker walls have been found to provide more realistic initial imperfection mode shapes [18,27]. A further justification for using a consistent imperfection shape for the same aspect ratio is that EHS members with the same aspect ratio but of different thicknesses are formed using the same fabrication process, which would be expected to lead to similar initial imperfection shapes [18]. The imperfection amplitudes Δw are calculated using

an expression from Annex D of EN 1993-1-6 [34] for circular shells, adapted for use with elliptical shells. The modified form of the expression is:

$$\Delta w = \frac{t}{Q}\sqrt{\frac{r_{eq}}{t}} \tag{9}$$

where r_{eq} is the equivalent radius = D_{eq} / 2 and Q is a fabrication quality parameter. Imperfection amplitudes are calculated based on D_{eq} set equal to $2a^2/b$ in order to maintain similar levels of imperfection for tubes bent about either the major axis or the minor axis. Figure 3 shows three different levels of imperfection amplitude calculated for the range of EHS currently considered, namely $\Delta w = 0.1t$, Δw from Eq.(5) with $Q = 40$ (Class A – excellent quality), and Δw from Eq.(7) with $Q = 25$ (Class B – high quality), plotted against the local buckling slenderness $\bar{\lambda}_\ell$. It was found previously [18] that the Class A level of imperfection amplitude provides an upper bound to measured values [5,6] and can be assumed to represent a level of imperfection amplitude suitable for the design of hot-finished EHS. The Class B level of imperfection amplitude was found to be onerously large, and is disregarded from the present study. Imperfection amplitudes equal to $0.1t$ can become unrealistically small; however, EHS containing such imperfections are included in the parametric study in order to demonstrate imperfection sensitivity when compared to EHS with more realistic Class A imperfections.

2.2 Validation of the numerical model

In order to confirm the accuracy of the numerical model, comparisons were made between the numerical predictions of ultimate moment with the results from previous experiments [6] on hot-finished EHS tubes bent about either the major axis or minor axis. The three specimens with $D_{eq}/t\varepsilon^2 > 140$ bent about their minor axis in four point bending (and thus with a constant bending moment across the central segment, which aids direct comparison with the simulations made herein under uniform moment) were selected, while the most slender specimen bent about its major axis was also selected; the aspect ratio of all the selected specimens was 2.0. The properties of the selected specimens are summarized in Table 1. Values of modulus of elasticity E and yield strength f_y obtained from tensile coupon testing [6] were applied in the numerical models. Since the nominal aspect ratio of the specimens simulated in the validation study is 2.0, the length of the specimens was set at 1200 mm in order to minimize length effects (see Section 3.1). Following the procedure described in Section 2.1.3, a mode shape was

extracted from linear eigenvalue analysis for each specimen and employed as the initial imperfection shape in a subsequent Riks analysis, with the imperfection amplitude Δw set equal to the values measured by [6], which are shown in Table 1.

In Figure 4, comparison is made between graphs of applied moment M against curvature χ obtained from the experiments [6] and those predicted by the numerical analysis; the curvature of the numerical specimens is taken as the average across the specimens and is defined as:

$$\chi = \theta / L \tag{10}$$

where θ is the relative rotation of the ends of the EHS specimen under uniform bending. Overall, good agreement can be observed between the experimental and numerical response for initial linear stiffness, the ultimate moment and the postbuckling behaviour; the ultimate moment of specimen 400 × 200 × 8.0 – B1 was reported [6] to be anomalously low, thus leading to the discrepancy observed in Figure 4a. The discrepancy between the experimental and numerical postbuckling equilibrium paths observed in Figure 4c is attributed to the choice of geometric imperfection shape and magnitude. In Table 2, comparison is made between the numerical $M_{u,FE}$ and the experimental $M_{u,exp}$ ultimate moments. It can be seen that there is close agreement between the two sets of results, again noting the anomalously low experimental ultimate moment reported by [6] for specimen 400 × 200 × 8.0 – B1.

In addition, comparison is also made between the numerical results for the ultimate moment obtained using the approach of modelling the tube under uniform moment and of modelling the tube under four point bending, $M_{u,4PB}$ [6]. As can be seen, there is very close agreement between the results, confirming that the simpler uniform moment models can be used in the parametric study.

3 NUMERICAL PARAMETRIC STUDY

Having shown that good agreement exists between the ultimate moments predicted by the numerical model and the results of [6], a parametric study was conducted in order to examine the influence of a number of key variables. In this section, the parameters varied in the study and the subsequent results obtained are presented and discussed.

3.1 Parameters for numerical studies

Four different aspect ratios are considered in the parametric study, namely, a/b = 1.5, 2.0, 3.0 and 5.0. The reference geometry is based on the commercially-available 300 × 150 series of elliptical sections with a/b = 2.0. The cross-sectional geometry for the other aspect ratios is based on maintaining a constant perimeter P = 726.3 mm. It was found previously that length

effects reduce in EHS with higher aspect ratios [3]; this is reflected by the simulated lengths of EHS tubes with a/b = 1.5 and 2.0 being set to 1200 mm, while those of EHS tubes with a/b = 3.0 and 5.0 were set to 1000 mm. Failure via global lateral torsional buckling was precluded owing to the definition of such short tube lengths.

In total, 240 cases were simulated in the parametric study, representing two axes of bending × four aspect ratios × five wall thicknesses × three yield strengths × two imperfection classes. In order to cover a wide range of local buckling slendernesses, the values of yield strength f_y and wall thickness t considered were extended outside the practical range, in keeping with [18]. The values of the cross-sectional dimensions, tube length L and yield strength f_y corresponding to the various aspect ratios a/b modelled are shown in Table 3, while the wall thicknesses t and imperfection amplitudes Δw applied in the parametric study are summarized in Table 4, while relevant properties of the specimens are shown in Tables 5 and 6 for specimens bent about the major axis and the minor axis, respectively.

3.2 Predicted failure modes

In this section, the failure modes predicted by the numerical models are discussed.

3.2.1 Major axis bending

Examples of failure modes observed in EHS specimens with Class A imperfections bent about the major axis are shown in Figure 5. For EHS with a/b = 1.5 and of lower slendernesses, the failure mechanism was a superposition of circumferential rucking and folding initiating at the critical radius (see Figure 5a); with increasing slenderness, circumferential rucking was less prevalent with the mode becoming more dominated by folding at the critical radius. For EHS with a/b = 2.0, the failure mode mainly involved folding at the critical radius, although some evidence of circumferential rucking at the extreme of the major axis was observed in thicker sections (see Figure 5b). For a/b = 3.0 (see Figure 5c), folding at the critical radius was the dominant mode, with circumferential rucking observable only in the least slender specimens. For EHS with a/b = 5.0 (see Figure 5d), folding initiating at the critical radius was the only mode observed. These failures modes are similar to those observed in [35]. In all specimens where folding at the critical radius was observed, the location of the point of initiation of buckling agreed well with the predication of the critical radius $r_{cr} = 0.4a^2/b$ in [6].

3.2.2 Minor axis bending

Examples of failure modes observed in EHS specimens with Class A imperfections bent about the minor axis are shown in Figure 6. For EHS with a/b = 1.5, failure tended to occur via

folding initiating at the minimum radius, although with some localized crumpling occurring in the less slender EHS (see Figure 6a). For EHS with $a/b \geq 2.0$ (see Figures 6b–d), folding at the minimum radius was the dominant mode; some evidence of the Yoshimura mechanism, which is more readily apparent in cylindrical shells in compression [36], was observed in particularly slender specimens with $a/b = 5.0$.

3.3 Moment–curvature behaviour

Graphs of moment M against curvature χ predicted by the numerical models are shown in Figures 7 and 8 for EHS bent about the major axis and the minor axis, respectively. Specimens with midrange slendernesses were chosen to facilitate comparison in Figures 7 and 8; as can be seen, the postbuckling stability of specimens decreased with increasing slenderness for all aspect ratios. For lower aspect ratios, the postbuckling response is observed to be less stable and more sensitive to imperfections. With increasing aspect ratio, the stability of the postbuckling response is increased with less imperfection sensitivity being observed. These trends are analogous to those observed previously for EHS in pure compression [18].

3.4 Strength reduction

In this section, the reduction in the ultimate moment M_u predicted by the numerical models relative to the elastic moment M_{el} is discussed. The reduction in resistance is characterized by the local buckling reduction factor $\rho = M_u / M_{el}$. Based on this definition, the factor ρ is equivalent to W_{eff} / W_{el} for slender sections, where W_{eff} is the effective section modulus, and thus specimens with $\rho < 1$ are slender, whereas those with $\rho \geq 1$ are fully-effective. In the following discussion, values for ρ calculated based on the results of the parametric study are compared with the elastic buckling curve:

$$\rho = \frac{1}{\bar{\lambda}_\ell^2}, \tag{11}$$

the Winter curve for plate buckling, adopted in EN 1993-1-5 [37], which is given by:

$$\rho = \begin{cases} 1 & \text{for} \quad \bar{\lambda}_\ell \leq 0.673 \\ \dfrac{1}{\bar{\lambda}_\ell} - \dfrac{0.22}{\bar{\lambda}_\ell^2} & \text{for} \quad \bar{\lambda}_\ell > 0.673 \end{cases} \tag{12}$$

and a power law design curve proposed by [6]:

$$\rho = \left(\frac{140 t \varepsilon^2}{D_{eq}} \right)^{0.25} = \left(\frac{\bar{\lambda}_0}{\bar{\lambda}_\ell} \right)^{0.5} \tag{13}$$

Eq.(13) is anchored to the width-to-thickness limit for slender EHS of $D_{eq}/t\varepsilon^2 = 140$ that is proposed [6] for inclusion in the upcoming revision to EN 1993-1-1 [20], so that sections with $\bar{\lambda}_\ell \leq \bar{\lambda}_0$, where $\bar{\lambda}_0 = 0.360$ for $E = 210000$ N/mm^2, are predicted to be fully-effective. It has also been proposed that Eq.(13) can be applied to EHS with $D_{eq}/t\varepsilon^2 \leq 240$, which is equivalent to $\bar{\lambda}_\ell \leq 0.471$ for $E = 210000$ N/mm^2. The suitability of this proposal is discussed herein, while additional proposed design curves that extend the range of applicability beyond this limit are also discussed in Section 4.1. The ultimate moments and resulting local buckling reduction factors obtained are shown in Tables 5 and 6 for specimens bent about the major axis and the minor axis, respectively.

3.4.1 Major axis bending

Values of ρ for EHS bent about the major axis are plotted against the local slenderness $\bar{\lambda}_\ell$ in Figures 9 to 12 for $a/b = 1.5$, $a/b = 2.0$, $a/b = 3.0$ and $a/b = 5.0$, respectively; these results are also compared with the elastic buckling curve, the Winter curve, Eq.(13) and the proposed design curve for $D_{eq} / t\varepsilon^2 > 240$ described in Section 4.1.

Upon review of the results of the parametric study, it can be seen that, overall, the moment resistance reduces and the imperfection sensitivity decreases with increasing slenderness, which is in accordance with similar behaviour observed by [18] for slender EHS in compression. It can also be seen that the elastic buckling curve, which is defined based on the critical buckling stress of circular shells (or elliptical shells through the use of the equivalent diameter D_{eq}) in pure compression, tends to provide an upper bound for EHS with Class A imperfections. For EHS with $\Delta w = 0.1t$ and of high slenderness, values of ρ exceed the elastic buckling curve and tend towards the Winter curve for plate buckling.

The levels of imperfection sensitivity predicted by the numerical parametric study for EHS with various aspect ratios are shown in Figure 13 by plotting ratios of the ultimate moment predicted with $\Delta w = 0.1t$, $M_{u,0.1t}$, to the ultimate moment predicted with Class A imperfections, $M_{u,A}$, against $\bar{\lambda}_\ell$. While a clear trend is not readily observable, in general, the imperfection sensitivity decreases with increasing aspect ratio.

It should be noted that the local buckling reduction factor ρ is greater than unity for a number of specimens with $D_{eq}/t\varepsilon^2 > 140$, indicating non-slender behaviour even for some Class 4 sections. It can be seen that Eq.(13) is safe-sided for low to mid-range slendernesses, while the

design curve proposed in the present work to extend the EHS moment resistance predictions beyond $D_{eq}/t\varepsilon^2 = 240$ provides safe-sided results for EHS with higher slendernesses.

3.4.2 Minor axis bending

Values of ρ for EHS bent about the minor axis are plotted against the local slenderness $\bar{\lambda}_\ell$ in Figures 14 to 17 for a/b = 1.5, a/b = 2.0, a/b = 3.0 and a/b = 5.0, respectively, with comparison made to the elastic buckling curve, the Winter curve, Eq.(13) and the proposed design curve described in Section 4.1. It can be seen that there is a trend of increasing stability, and hence local buckling resistance, with increasing aspect ratio, as well as a trend of decreasing imperfection sensitivity with increasing aspect ratio. It can also be seen that the elastic buckling curve provides an upper bound for all results.

In Figure 18, the imperfection sensitivity is shown for the range of EHS examined; the trend of decreasing imperfection sensitivity with increasing aspect ratio is more clearly apparent than for EHS being bent about the major axis. As was observed for EHS bent about the major axis, Eq.(13) provides safe-sided resistance predictions for EHS of low to mid-range slendernesses, while the proposed extension to this design curve is also safe for use with EHS with higher slendernesses.

4 DESIGN GUIDANCE

In this section, design curves are proposed that extend the range of applicability of the proposals of [6] and the upcoming revision to EN 1993-1-1 [20] beyond $D_{eq}/t\varepsilon^2 = 240$. A reliability analysis of the design proposal presented in Section 4.1, in addition to proposed design rules for Class 4 EHS in compression [20], is also described.

4.1 Design proposal

Although buckling resistance is also a function of imperfection amplitude, the curves described in this section are calibrated based on the more realistic Class A level of imperfection. The rules are adapted from Eq.(13) and have been fitted to provide lower bounds to the results of the parametric study. The proposed design formulae are given in Eq.(14), which are applicable to EHS in bending with $\bar{\lambda}_\ell \leq 1.7$. As mentioned in Section 2.1.1, this encompasses the practical range of EHS geometries and material properties. The curve is equivalent to Eq.(13) up to a limiting slenderness $\bar{\lambda}_1$; the local buckling reduction factor ρ is given by:

$$\rho = \begin{cases} 1 & \text{for} \quad \bar{\lambda}_\ell \le \bar{\lambda}_0 \\ \left(\dfrac{\bar{\lambda}_0}{\bar{\lambda}_\ell}\right)^{0.5} & \text{for} \quad \bar{\lambda}_0 < \bar{\lambda}_\ell \le \bar{\lambda}_1 \\ \left(\dfrac{\bar{\lambda}_0}{\bar{\lambda}_1}\right)^{0.5}\left(\dfrac{\bar{\lambda}_1}{\bar{\lambda}_\ell}\right)^{\beta} & \text{for} \quad \bar{\lambda}_\ell > \bar{\lambda}_1 \end{cases} \tag{14}$$

where values for the parameters $\bar{\lambda}_0$, $\bar{\lambda}_1$ and β can be found in Table 7.

The resulting design curves are shown in Figures 19 and 20 for EHS bent about the major axis and the minor axis, respectively. It can be seen that the design curves provide safe lower bounds to the results of the parametric study. In addition, the increase in postbuckling stability with increasing aspect ratio is also observable.

Ratios of the ultimate moment obtained from numerical analysis, $M_{u,FE}$, to the predicted design ultimate moment, $M_{u,D}$, are shown in Figures 21 and 22 for EHS bent about the major axis and the minor axis, respectively. It can be seen that the design curves tend to provide safe-sided predictions for the ultimate moment, i.e., the ratios are greater than unity, for all aspect ratios, while also not being overly conservative. It can be seen that the design predictions in the low slenderness range tend to be more conservative; this is due to the value of the plateau slenderness $\bar{\lambda}_0$ being fixed equal to 0.360 for all aspect ratios in order to maintain compatibility with the limit of $D_{eq}/t\varepsilon^2 = 140$ proposed by EN 1993-1-1 [20]. The trend of increasing local buckling resistance with increasing aspect ratio is also reflected by the increased values of $M_{u,FE}$ / $M_{u,D}$ for higher aspect ratios in both Figure 21 and Figure 22.

4.2 Reliability analysis

In this section, a reliability analysis is conducted to determine the required partial factor for cross-sectional resistance γ_{M0} in accordance with EN 1990 [28] Annex D for the design of slender EHS. Required partial factors are determined: for: Case 1 – Eq.(13) for the design of slender EHS in bending with $D_{eq}/t\varepsilon^2 \le 240$; Case 2 – Eq.(12) for the design of slender EHS in bending with $D_{eq}/t_e^2 > 240$; Case 3 – Eq.(15) [5] for the design of slender EHS in compression with $D_{eq}/t\varepsilon^2 \le 240$.

$$\rho = \left(\frac{90t\varepsilon^2}{D_{eq}}\right)^{0.5} \tag{15}$$

It should be noted that Eq.(15) is intended for application to EHS with $D_{eq}/t\varepsilon^2 \leq 240$, but in the present study, the use of this function is also assessed beyond this limit across the full range of specimens considered in [18]. Demonstrating that the required partial factors for these methods are less than or equal to unity supports their proposed use within the Eurocode framework with a partial factor $\gamma_{M0} = 1.00$.

A first-order reliability method (FORM) similar to that used for concrete-filled EHS columns [12], hot-rolled steel sections [38] and stainless steel sections [39–41] was employed in the present study; a detailed description of the theoretical background of the methodology can be found in [39,42]. The general form of the resistance function r_t for slender EHS in either bending or compression is:

$$r_t = \rho X f_y \tag{16}$$

where X is the cross-sectional geometric property relevant to the loading mode, which is the major axis elastic modulus $W_{el,y}$ for sections bent about the major axis, the minor axis elastic modulus $W_{el,y}$ for sections bent about the minor axis and the cross-sectional area A for sections in compression; based on this definition, the effective area of a slender EHS in compression can be taken as $A_{eff} = \rho A$.

The coefficient of variation of the errors between the design predictions and the observed numerical resistances, V_δ, as defined in Annex D of EN 1990 [28] is dependent on the slope b_r between the observed numerical resistances r_e and theoretical design resistances r_t, which is given by:

$$b_r = \frac{1}{n}\sum \frac{r_{e,i}}{r_{t,i}} \tag{17}$$

where n is the number of specimens considered for a particular design method. Note that this definition of b_r reduces the bias in favour of specimens with higher observed resistances [38] when compared to the least-squares definition of b_r found in EN 1990 Annex D [28]. The coefficient of variation of the material yield strength V_{fy} is set to 0.055 [20,41]. For EHS members, the variance of the geometric properties should consider the variances of the dimensions of the major axis diameter, minor axis diameter and the tube wall thickness, the coefficients of variation of which are 0.009, 0.009 and 0.025, respectively [20]. Given that these variances are small, a close approximation for the combined coefficient of variation of the geometric properties can be found from the root of the sum of the squares of the dimensional variances, which yields $V_g = 0.028$. The combined coefficient of variation of the resistances V_r for a particular design method is then found from:

$$V_{\mathrm{r}}^2 = (V_\delta^2 + 1)(V_{fy}^2 + 1)(V_{\mathrm{g}}^2 + 1) - 1 \tag{16}$$

The required partial factor for a given design method is defined as $\gamma_{M0} = r_n / r_d$, where r_n is the nominal resistance and r_d is the design resistance. Adopting the approach of EN 1990 [28], the design resistance is determined using mean values for the design variables, while in keeping with the approach employed by [39,40], the nominal resistance r_n is determined using nominal values of the design variables. Thus, the definition of γ_{M0} contains the ratio of the mean yield strength to the nominal yield strength $f_{y,mean} / f_{y,nom}$, which for mild steel grades can be taken as 1.25 [20,38,42].

The reliability analysis is configured on the basis of achieving a target reliability index $\beta > 3.8$, which is equivalent to a probability of failure of less than 1×10^{-4} across a reference period of 50 years; this level of reliability is ensured through the use of appropriate design fractile factors (for the ultimate limit state) $k_{d,n}$.

The parameters used when conducting the reliability analyses and the resulting required partial factors are shown in Table 8. Sections in bending with $D_{eq}/t\varepsilon^2 < 140$ and sections in compression with $D_{eq}/t\varepsilon^2 < 90$ were omitted from the analysis since the design methods investigated are not applicable in these ranges; the discrepancy between the numbers of specimens considered in major axis bending and in minor axis bending is due to the difference in definition of D_{eq} and also when considering specimens with $\bar{\lambda}_\ell \leq 1.7$. As can be seen, the partial factors for all the considered design methods are less than or close to unity, indicating that the value of $\gamma_{M0} = 1.00$ recommended in EN 1993-1-1 [20] is appropriate for use in the design of Class 4 EHS in either bending or compression.

5 CONCLUSIONS

The local buckling of slender elliptical hollow sections (EHS) in bending has been investigated using numerical methods. The numerical model was validated against previous experimental results with good agreement observed, after which an extensive parametric study was conducted. The parametric study comprised simulations of EHS bent about either the major axis or minor axis, with cross-section aspect ratios ranging from 1.5 to 5.0, nondimensional local buckling slendernesses ranging from 0.25 to 2.15 and wall thicknesses from 0.7 mm to 8.7 mm. Two different imperfection classes were considered: $\Delta w = 0.1t$ and Class A imperfections.

For EHS bent about the major axis with lower aspect ratios, circumferential rucking was the predominant failure mode, while for EHS with higher aspect ratios, the failure mode transitioned to folding at the critical radius. For EHS bent about the minor axis, folding initiating at the extreme of the minor axis was observable for all aspect ratios, with some crumpling being observed in EHS with a/b = 1.5, while the Yoshimura mechanism [36] was also observed in some EHS specimens with a/b = 5.0. Upon examination of the results for ultimate moment and moment–curvature behaviour, trends of increasing postbuckling stability and decreasing imperfection sensitivity with increasing aspect ratio were observed, in keeping with analogous behaviour observed in slender EHS in compression.

A design method has been proposed for Class 4 EHS members that extends the range of applicability of design rules that are to be included in the upcoming revision to EN 1993-1-1 [20]. The proposals were shown to provide safe-sided and accurate predictions for the moment resistance of EHS with nondimensional local slendernesses $\bar{\lambda}_\ell \leq 1.7$ and aspect ratios from 1.5 to 5.0. A reliability analysis of design methods for EHS in bending or compression, including provisions that are to be included in the upcoming revision to EN 1993-1-1 [20] showed that using a partial safety factor for cross-sectional resistance γ_{M0} = 1.00 is appropriate for all the design methods considered and leads to safe-sided design predictions of the respective ultimate resistances.

REFERENCES

[1] Comité Européen de Normalisation. *EN 10210-1:2006 Hot finished structural hollow sections of non-alloy and fine grain steels – Part 1: Technical delivery conditions*. British Standards Institution, 2006.

[2] Chan TM, Gardner L, Law KH. Structural design of elliptical hollow sections: a review. *Proceedings of the Institution of Civil Engineers – Structures and Buildings* 2010;163(6):391-402.

[3] Ruiz-Teran AM, Gardner L. Elastic buckling of elliptical tubes. *Thin-Walled Structures* 2008;46(11):1304–1318.

[4] Gardner L, Chan TM. Cross-section classification of elliptical hollow sections. *Steel and Composite Structures* 2007;7(3):185–200.

[5] Chan TM, Gardner L. Compressive resistance of hot-rolled elliptical hollow sections. *Engineering Structures* 2008;30(2):522–532.

[6] Chan TM, Gardner L. Bending strength of hot-rolled elliptical hollow sections, *Journal of. Constructional Steel Research* 2008;64(9):971–986.

[7] Silvestre N. Buckling behaviour of elliptical cylindrical shells and tubes under compression, *International Journal of Solids and Structures* 2008;45(16):4427–4447.

[8] Chan TM, Gardner L. Flexural buckling of elliptical hollow section columns, *Journal of Structural Engineering ASCE* 2009;135(5):546–557.

[9] Theofanous M, Chan TM, Gardner L. Structural response of stainless steel oval hollow section compression members, *Engineering Structures* 2009;31(4):922–34.

[10] Scullion T, Ali F, Nadjai A. Experimental study on performance of elliptical section steel columns, under hydrocarbon fire, *Journal of Constructional Steel Research* 2011;67:986–991.

[11] McCann F, Gardner L, Qiu W. Experimental study of slender concrete-filled elliptical hollow section beam-columns, *Journal of Constructional Steel Research* 2015;113:185–194.

[12] Qiu W., McCann, F., Espinos, A., Romero, M.L., Gardner, L. Numerical analysis and design of slender concrete-filled elliptical hollow section columns and beam-columns, *Engineering Structures*, 131:90–100.

[13] Espinos, A., Romero, M. L., Portolés, J, M. and Hospitaler, A. 2014. Ambient and fire behavior of eccentrically loaded elliptical slender concrete-filled tubular columns. *Journal of Constructional Steel Research*, 100, 97–107.

[14] Sheehan, T, Dai, X. H., Chan, T. M., Lam, D. Structural response of concrete-filled elliptical steel hollow sections under eccentric compression. *Engineering Structures* 2012*;*45:314–323.

[15] Theofanous M, Chan TM, Gardner L. Flexural behaviour of stainless steel oval hollow sections. *Thin-Walled Structures* 2009;47(6-7):776-787.

[16] Law KH, Gardner L. Buckling of elliptical hollow section members under combined compression and uniaxial bending, *Journal of Constructional Steel Research* 2013;86:1–16.

[17] Gardner L, Chan TM, Wadee MA. Shear response of elliptical hollow sections, *Proceedings of the Institution of Civil Engineers – Structures and Buildings* 2008;161(6):301–309.

[18] McCann F, Fang C, Gardner L, Silvestre N. Local buckling and ultimate strength of slender elliptical hollow sections in compression. *Engineering Structures*, 111:104–118.

[19] Steel Construction Institute. *Steel building design: Design data*. Publication Number P363. Steel Construction Institute 2013.

[20] Comité Européen de Normalisation. *prEN 1993-1-1:2018 Final Draft - Eurocode 3 - Design of steel structures, Part 1.1: General rules and rules for buildings*, CEN, 2018.

[21] Zhu JH, Young B. Design of cold-formed steel oval hollow section columns, *Journal of Constructional Steel Research* 2012;71:26–37.

[22] Gardner L, Saari N, Wang F. Comparative experimental study of hot-rolled and cold-formed rectangular hollow sections, *Thin-Walled Structures* 2010;48(7):495-507.

[23] Jandera M, Gardner L, Machacek J. Residual stresses in cold-rolled stainless steel hollow sections, *Journal of Constructional Steel Research,* 2008;64(11):1255–1263.

[24] Kempner J, Chen YN. Large deflections of an axially compressed oval cylindrical shell, *Proceedings of the 11th International Congress of Applied Mechanics*, Munich, 1964.

[25] Tennyson RC, Booton M, Caswell RD. Buckling of imperfect elliptical cylindrical shells under axial compression, *AIAA Journal* 1971;9(2):250–5.

[26] Feinstein G, Erickson B, Kempner J. Stability of oval cylindrical shells. *Experimental Mechanics*,1971;11(11):514–20.

[27] Silvestre, N., Gardner, L. Elastic local postbuckling of elliptical tubes, *Journal of Constructional Steel Research* 2011;67(3):281–292.

[28] Comité Européen de Normalisation. *EN 1990:2002 Eurocode – Basis of structural design*, CEN, 2002.

[29] ABAQUS. *ABAQUS Analysis User's manual, v6.12.3*, USA: Dassault Systems Simulia Corp., Providence; 2012.

[30] Gerard, G., Becker, H. Handbook of structural stability: Part III – Buckling of curved plates and shells. Technical note 3783, NACA, 1957.

[31] Abela, J.M., Gardner, L. Elastic buckling of elliptical tubes subjected to generalised linearly varying stress distributions, *Thin-Walled Structures* 2012;58:40–50.

[32] Ma, J.-L., Chan, T.-M., Young, B. 2017. Tests of high-strength steel hollow sections: a review, *Proceedings of the Institution of Civil Engineers – Structures and Buildings*, 170(9):621–630.

[33] Müller, T., Straetmans, B. 2015 High strength seamless tubes and steel hollow sections for crane and machine building applications, *Stahlbau*, 84(9):650–654.

[34] Comité Européen de Normalisation. *EN 1993-1-6:2007 Eurocode 3 - Design of steel structures, Part 1-6: Strength and stability of shell structures*, CEN, 2007.

[35] Insausti A, Gardner L. 2011. Analytical modelling of plastic collapse in compressed elliptical hollow sections. *Journal of Constructional Steel Research,* 67:678–89.

[36] Yoshimura, Y. 1955. On the mechanism of buckling of a circular cylindrical shell under axial compression. National Advisory Committee for Aeronautics Technical Memorandum 1390. NACA, 1955.

[37] Comité Européen de Normalisation. *EN 1993-1-5:2006 Eurocode 3 - Design of steel structures, Part 1-5: Plated structural elements*, CEN, 2006.

[38] Yun X, Gardner L, Boissonade N. 2018. The continuous strength method for the design of hot-rolled steel cross-sections. *Engineering Structures*, 157:179–191.

[39] Afshan S, Francis P, Baddoo, NR, Gardner L. 2015. Reliability analysis of structural stainless steel design provisions. *Journal of Constructional Steel Research,* 114:293–304.

[40] Afshan S, Zhao O, Gardner L. 2019. Standardised material properties for numerical parametric studies of stainless steel structures and buckling curves for tubular columns. *Journal of Constructional Steel Research*, 152:2–11.

[41] Liang Y, Zhao O, Long Y-L, Gardner L. 2019. Stainless steel channel sections under combined compression and minor axis bending – Part 2: Parametric studies and design. *Journal of Constructional Steel Research,* 152:162–172.

[42] Tankova T, Simoes da Silva L, Marques L, Rebelo C, Taras A. 2014. Towards a standardized procedure for the safety assessment of stability design rules. *Journal of Constructional Steel Research*, 103:290–302.

Table 1: Measured properties of specimens used in validation of numerical model [6].

Specimen	Axis of bending	$2a$ (mm)	$2b$ (mm)	t (mm)	Δw (mm)	E (N/mm^2)	f_y (N/mm^2)	$D_{eq}/t\varepsilon^2$
400 × 200 × 8.0 – B1	Minor	396.09	207.63	7.75	0.43	221600	429	178
400 × 200 × 10.0 – B1	Minor	396.06	207.54	9.65	1.14	197100	401	134
500 × 250 × 8.0 – B1	Minor	495.34	255.85	7.78	2.01	223800	413	217
500 × 250 × 8.0 – B2	Major	491.74	260.92	7.78	0.47	223800	413	83.7

Table 2: Comparison of numerical and experimental results.

Specimen	$M_{u,FE}$ (kNm)	$M_{u,exp}$ (kNm)	$M_{u,FE}$ / $M_{u,exp}$	$M_{u,FE}$ / $M_{u,4PB}$
400 × 200 × 8.0 - B1	210	186	1.13	1.01
400 × 200 × 10.0 - B1	238	232	1.02	1.00
500 × 250 × 8.0 - B1	291	291	1.00	1.03
500 × 250 × 8.0 - B2	511	497	1.03	0.99
Average			1.05	1.01
Standard deviation			0.06	0.02

Table 3: Aspect ratios used in numerical parametric study with corresponding cross-sectional dimensions, yield strengths and tube lengths.

Aspect ratio a/b	$2a$ (mm) × $2b$ (mm)	Length L (mm)	Values of f_y (N/mm^2)
1.5	274.8 × 183.2	1200	390.6, 1200, 2500
2.0	300 × 150	1200	390.6, 900, 1800
3.0	326 × 108.8	1000	390.6, 700, 1150
5.0	346 × 69.2	1000	390.6, 500, 700

Table 4: Geometric properties varied in numerical parametric study.

Parameter	Values assumed in parametric study
Wall thickness *t* (mm)	0.7[1], 1.0, 1.5, 2.1, 4.2, 8.7[2]
Imperfection amplitudes	0.1*t*, Class A

[1] Major axis bending only.

[2] Minor axis bending only.

Table 5: Geometric properties, design parameters and moments of resistance of specimens bent about the major axis.

Aspect ratio	$2a$ (mm)	$2b$ (mm)	t (mm)	f_y (N/mm^2)	Δw (mm)		$D_{eq} / t\varepsilon^2$	f_{cr} (N/mm^2)	$\overline{\lambda}_\ell$	$W_{el,y}$ (mm^3)	$M_{el,y}$ (kNm)	M_u (kNm)	
					$\Delta w = 0.1t$	Class A						$\Delta w = 0.1t$	Class A
a/b = 1.5	274.8	183.2	4.2	390.6	0.42	0.74	65.3	6475	0.246	179784	70.2	93.9	93.2
	274.8	183.2	2.1	390.6	0.21	0.52	130.5	3238	0.347	92220	36.0	43.7	43.5
	274.8	183.2	1.5	390.6	0.15	0.44	182.7	2313	0.411	66352	25.9	29.8	29.7
	274.8	183.2	1.0	390.6	0.10	0.36	274.1	1542	0.503	44503	17.4	18.2	18.8
	274.8	183.2	0.7	390.6	0.07	0.30	391.5	1079	0.602	31265	12.2	12.2	12.5
	274.8	183.2	4.2	1200	0.42	0.74	200.5	6475	0.430	179784	215.7	266.4	265.5
	274.8	183.2	2.1	1200	0.21	0.52	400.9	3238	0.609	92220	110.7	110.9	114.0
	274.8	183.2	1.5	1200	0.15	0.44	561.3	2313	0.720	66352	79.6	77.6	77.9
	274.8	183.2	1.0	1200	0.10	0.36	841.9	1542	0.882	44503	53.4	51.1	42.0
	274.8	183.2	0.7	1200	0.07	0.30	1202.8	1079	1.054	31265	37.5	29.9	22.5
	274.8	183.2	4.2	2500	0.42	0.74	417.6	6475	0.621	179784	449.5	474.2	470.6
	274.8	183.2	2.1	2500	0.21	0.52	835.3	3238	0.879	92220	230.6	210.0	163.5
	274.8	183.2	1.5	2500	0.15	0.44	1169.4	2313	1.040	66352	165.9	129.6	86.8
	274.8	183.2	1.0	2500	0.10	0.36	1754.0	1542	1.273	44503	111.3	59.1	42.0
	274.8	183.2	0.7	2500	0.07	0.30	2505.8	1079	1.522	31265	78.2	29.9	22.5
a/b = 2.0	300.0	150.0	4.2	390.6	0.42	0.89	95.0	4448	0.296	183192	71.6	97.0	95.9
	300.0	150.0	2.1	390.6	0.21	0.63	190.0	2224	0.419	93892	36.7	45.0	45.4
	300.0	150.0	1.5	390.6	0.15	0.53	265.9	1589	0.496	67539	26.4	30.8	31.0
	300.0	150.0	1.0	390.6	0.10	0.43	398.9	1059	0.607	45290	17.7	19.4	19.2
	300.0	150.0	0.7	390.6	0.07	0.36	569.9	741	0.726	31814	12.4	13.2	13.1
	300.0	150.0	4.2	900	0.42	0.89	218.8	4448	0.450	183192	164.9	209.4	208.0
	300.0	150.0	2.1	900	0.21	0.63	437.7	2224	0.636	93892	84.5	92.2	91.2
	300.0	150.0	1.5	900	0.15	0.53	612.8	1589	0.753	67539	60.8	63.3	62.8
	300.0	150.0	1.0	900	0.10	0.43	919.1	1059	0.922	45290	40.8	40.8	29.1
	300.0	150.0	0.7	900	0.07	0.36	1313.1	741	1.102	31814	28.6	27.3	14.7
	300.0	150.0	4.2	1800	0.42	0.89	437.7	4448	0.636	183192	329.7	380.4	375.3
	300.0	150.0	2.1	1800	0.21	0.63	875.4	2224	0.900	93892	169.0	167.4	133.2
	300.0	150.0	1.5	1800	0.15	0.53	1225.5	1589	1.064	67539	121.6	115.7	65.5
	300.0	150.0	1.0	1800	0.10	0.43	1838.3	1059	1.304	45290	81.5	54.9	29.1
	300.0	150.0	0.7	1800	0.07	0.36	2626.1	741	1.558	31814	57.3	27.4	14.7

a/*b* = 3.0	326.0	108.8	4.2	390.6	0.42	1.13	154.6	2732	0.378	183265	71.6	98.6	96.4
	326.0	108.8	2.1	390.6	0.21	0.80	309.3	1366	0.535	93853	36.7	47.0	45.2
	326.0	108.8	1.5	390.6	0.15	0.68	433.0	976	0.633	67496	26.4	30.9	30.9
	326.0	108.8	1.0	390.6	0.10	0.55	649.4	651	0.775	45253	17.7	19.7	17.5
	326.0	108.8	0.7	390.6	0.07	0.46	927.8	455	0.926	31785	12.4	13.3	9.1
	326.0	108.8	4.2	700	0.42	1.13	277.1	2732	0.506	183265	128.3	167.6	165.0
	326.0	108.8	2.1	700	0.21	0.80	554.2	1366	0.716	93853	65.7	75.5	72.2
	326.0	108.8	1.5	700	0.15	0.68	775.9	976	0.847	67496	47.2	51.5	39.2
	326.0	108.8	1.0	700	0.10	0.55	1163.8	651	1.037	45253	31.7	33.0	18.4
	326.0	108.8	0.7	700	0.07	0.46	1662.6	455	1.240	31785	22.2	18.7	9.1
	326.0	108.8	4.2	1150	0.42	1.13	455.2	2732	0.649	183265	210.8	268.9	252.7
	326.0	108.8	2.1	1150	0.21	0.80	910.5	1366	0.917	93853	107.9	115.4	89.5
	326.0	108.8	1.5	1150	0.15	0.68	1274.7	976	1.086	67496	77.6	79.0	45.3
	326.0	108.8	1.0	1150	0.10	0.55	1912.0	651	1.330	45253	52.0	37.8	19.8
	326.0	108.8	0.7	1150	0.07	0.46	2731.5	455	1.589	31785	36.6	18.8	11.1
a/*b* = 5.0	346.0	69.2	4.2	390.6	0.42	1.51	273.9	1543	0.503	181400	70.9	97.4	93.8
	346.0	69.2	2.1	390.6	0.21	1.07	547.7	771	0.712	92800	36.2	43.6	40.1
	346.0	69.2	1.5	390.6	0.15	0.90	766.8	551	0.842	66719	26.1	29.5	24.2
	346.0	69.2	1.0	390.6	0.10	0.74	1150.2	367	1.031	44721	17.5	18.4	10.3
	346.0	69.2	0.7	390.6	0.07	0.62	1643.1	257	1.232	31407	12.3	9.9	6.0
	346.0	69.2	4.2	500	0.42	1.51	350.6	1543	0.569	181400	90.7	119.1	116.8
	346.0	69.2	2.1	500	0.21	1.07	701.1	771	0.805	92800	46.4	54.2	46.9
	346.0	69.2	1.5	500	0.15	0.90	981.6	551	0.953	66719	33.4	34.7	24.9
	346.0	69.2	1.0	500	0.10	0.74	1472.3	367	1.167	44721	22.4	19.2	11.0
	346.0	69.2	0.7	500	0.07	0.62	2103.3	257	1.394	31407	15.7	9.9	6.6
	346.0	69.2	4.2	700	0.42	1.51	490.8	1543	0.674	181400	127.0	165.4	155.7
	346.0	69.2	2.1	700	0.21	1.07	981.6	771	0.953	92800	65.0	70.1	53.4
	346.0	69.2	1.5	700	0.15	0.90	1374.2	551	1.127	66719	46.7	41.1	27.4
	346.0	69.2	1.0	700	0.10	0.74	2061.3	367	1.380	44721	31.3	19.2	12.2
	346.0	69.2	0.7	700	0.07	0.62	2944.7	257	1.650	31407	22.0	9.87	7.3

Table 6: Geometric properties, design parameters and moments of resistance of specimens bent about the minor axis.

Aspect ratio	$2a$ (mm)	$2b$ (mm)	t (mm)	f_y (N/mm^2)	Δw (mm)		$D_{eq} / t\varepsilon^2$	f_{cr} (N/mm^2)	$\bar{\lambda}_\ell$	$W_{el,z}$ (mm^3)	$M_{el,z}$ (kNm)	M_u (kNm)	
					$\Delta w = 0.1t$	Class A						$\Delta w = 0.1t$	Class A
a/b = 1.5	274.8	183.2	8.7	390.6	0.87	1.06	78.8	5365	0.270	279081	109.0	148.9	148.2
	274.8	183.2	4.2	390.6	0.42	0.74	163.1	2590	0.388	144341	56.4	68.8	67.8
	274.8	183.2	2.1	390.6	0.21	0.52	326.3	1295	0.549	74489	29.1	30.7	30.2
	274.8	183.2	1.5	390.6	0.15	0.44	456.8	925	0.650	53686	21.0	21.0	20.8
	274.8	183.2	1.0	390.6	0.10	0.36	685.1	617	0.796	36058	14.1	13.7	13.6
	274.8	183.2	8.7	1200	0.87	1.06	240.0	5365	0.473	279081	334.9	426.7	424.4
	274.8	183.2	4.2	1200	0.42	0.74	501.2	2590	0.681	144341	173.2	174.0	169.0
	274.8	183.2	2.1	1200	0.21	0.52	1002.3	1295	0.963	74489	89.4	68.7	58.7
	274.8	183.2	1.5	1200	0.15	0.44	1403.2	925	1.139	53686	64.4	39.3	32.4
	274.8	183.2	1.0	1200	0.10	0.36	2104.9	617	1.395	36058	43.3	19.9	16.0
	274.8	183.2	8.7	2500	0.87	1.06	504.0	5365	0.683	279081	697.7	735.8	727.9
	274.8	183.2	4.2	2500	0.42	0.74	1044.1	2590	0.982	144341	360.9	228.4	212.0
	274.8	183.2	2.1	2500	0.21	0.52	2088.1	1295	1.389	74489	186.2	68.8	58.7
	274.8	183.2	1.5	2500	0.15	0.44	2923.4	925	1.644	53686	134.2	39.3	32.4
	274.8	183.2	1.0	2500	0.10	0.36	4385.1	617	2.013	36058	90.1	19.9	16.0
a/b = 2.0	300.0	150.0	8.7	390.6	0.87	1.28	114.6	3686	0.326	236534	92.4	125.8	124.5
	300.0	150.0	4.2	390.6	0.42	0.89	237.4	1779	0.469	123631	48.3	57.1	54.9
	300.0	150.0	2.1	390.6	0.21	0.63	474.9	890	0.663	64102	25.0	25.5	22.9
	300.0	150.0	1.5	390.6	0.15	0.53	664.9	635	0.784	46261	18.1	17.6	13.8
	300.0	150.0	1.0	390.6	0.10	0.43	997.3	424	0.960	31106	12.1	10.8	6.6
	300.0	150.0	8.7	900	0.87	1.28	264.1	3686	0.494	236534	212.9	263.7	265.1
	300.0	150.0	4.2	900	0.42	0.89	547.1	1779	0.711	123631	111.3	104.8	94.7
	300.0	150.0	2.1	900	0.21	0.63	1094.2	890	1.006	64102	57.7	37.2	27.1
	300.0	150.0	1.5	900	0.15	0.53	1531.9	635	1.190	46261	41.6	21.0	14.1
	300.0	150.0	1.0	900	0.10	0.43	2297.9	424	1.458	31106	28.0	10.9	7.1
	300.0	150.0	8.7	1800	0.87	1.28	528.2	3686	0.699	236534	425.8	444.8	428.3
	300.0	150.0	4.2	1800	0.42	0.89	1094.2	1779	1.006	123631	222.5	129.3	111.5
	300.0	150.0	2.1	1800	0.21	0.63	2188.4	890	1.422	64102	115.4	37.5	27.1
	300.0	150.0	1.5	1800	0.15	0.53	3063.8	635	1.683	46261	83.3	21.3	15.2
	300.0	150.0	1.0	1800	0.10	0.43	4595.7	424	2.061	31106	56.0	10.9	8.0

a/*b* = 3.0	326.0	108.8	8.7	390.6	0.87	1.63	186.6	2264	0.415	173555	67.8	94.6	93.2
	326.0	108.8	4.2	390.6	0.42	1.13	386.6	1093	0.598	92905	36.3	42.0	39.3
	326.0	108.8	2.1	390.6	0.21	0.80	773.1	546	0.845	48681	19.0	17.9	14.3
	326.0	108.8	1.5	390.6	0.15	0.68	1082.4	390	1.000	35235	13.8	11.0	7.9
	326.0	108.8	1.0	390.6	0.10	0.55	1623.6	260	1.225	23750	9.3	5.5	4.3
	326.0	108.8	8.7	700	0.87	1.63	334.4	2264	0.556	173555	121.5	161.7	157.6
	326.0	108.8	4.2	700	0.42	1.13	692.8	1093	0.800	92905	65.0	61.4	54.2
	326.0	108.8	2.1	700	0.21	0.80	1385.5	546	1.132	48681	34.1	19.5	14.7
	326.0	108.8	1.5	700	0.15	0.68	1939.7	390	1.339	35235	24.7	11.0	9.7
	326.0	108.8	1.0	700	0.10	0.55	2909.6	260	1.640	23750	16.6	5.5	5.3
	326.0	108.8	8.7	1150	0.87	1.63	549.4	2264	0.713	173555	199.6	233.4	224.8
	326.0	108.8	4.2	1150	0.42	1.13	1138.1	1093	1.026	92905	106.8	69.1	59.2
	326.0	108.8	2.1	1150	0.21	0.80	2276.2	546	1.451	48681	56.0	19.6	18.1
	326.0	108.8	1.5	1150	0.15	0.68	3186.7	390	1.716	35235	40.5	11.0	10.8
	326.0	108.8	1.0	1150	0.10	0.55	4780.1	260	2.102	23750	27.3	5.5	5.8
a/*b* = 5.0	346.0	69.2	8.7	390.6	0.87	2.17	330.5	1278	0.553	104400	40.8	60.1	56.0
	346.0	69.2	4.2	390.6	0.42	1.51	684.6	617	0.796	59007	23.0	22.1	18.9
	346.0	69.2	2.1	390.6	0.21	1.07	1369.3	309	1.125	31648	12.4	6.2	5.1
	346.0	69.2	1.5	390.6	0.15	0.90	1917.0	220	1.331	23055	9.0	3.3	2.6
	346.0	69.2	1.0	390.6	0.10	0.74	2875.5	147	1.630	15622	6.1	2.0	1.2
	346.0	69.2	8.7	500	0.87	2.17	423.1	1278	0.625	104400	52.2	74.1	68.1
	346.0	69.2	4.2	500	0.42	1.51	876.4	617	0.900	59007	29.5	24.5	21.2
	346.0	69.2	2.1	500	0.21	1.07	1752.8	309	1.273	31648	15.8	6.2	5.5
	346.0	69.2	1.5	500	0.15	0.90	2453.9	220	1.506	23055	11.5	3.3	2.8
	346.0	69.2	1.0	500	0.10	0.74	3680.9	147	1.845	15622	7.8	1.7	1.2
	346.0	69.2	8.7	700	0.87	2.17	592.3	1278	0.740	104400	73.1	94.8	85.7
	346.0	69.2	4.2	700	0.42	1.51	1227.0	617	1.065	59007	41.3	25.8	24.3
	346.0	69.2	2.1	700	0.21	1.07	2453.9	309	1.506	31648	22.2	6.2	6.0
	346.0	69.2	1.5	700	0.15	0.90	3435.5	220	1.782	23055	16.1	3.3	3.0
	346.0	69.2	1.0	700	0.10	0.74	5153.2	147	2.183	15622	10.9	1.7	1.3

Table 7: Summary of parameters applied in design curves.

Parameter	Major axis bending	Minor axis bending
β	1.45	2.00
$\overline{\lambda}_0$	0.360	
$\overline{\lambda}_1$	0.830	

Table 8: Reliability analysis parameters and required partial factors for the design of slender EHS in bending and compression.

	n	b_r	V_δ	V_r	$k_{d,n}$	γ_{M0}
Case 1 [6] – Eq.(13), $D_{eq}/t\varepsilon^2 \leq 240$						
- Major axis bending	10	1.343	0.054	0.082	4.510	0.81
- Minor axis bending	8	1.382	0.075	0.097	5.070	0.88
Case 2 – Eq.(14), $D_{eq}/t\varepsilon^2 > 240$						
- Major axis bending	104	1.548	0.196	0.206	3.077	0.98
- Minor axis bending	100	1.476	0.157	0.169	3.080	0.93
Case 3 [5] – Eq.(15)						
- $D_{eq}/t\varepsilon^2 \leq 240$	33	1.412	0.162	0.173	3.410	1.02
- $D_{eq}/t\varepsilon^2 > 240$	231	2.152	0.202	0.212	3.053	0.72

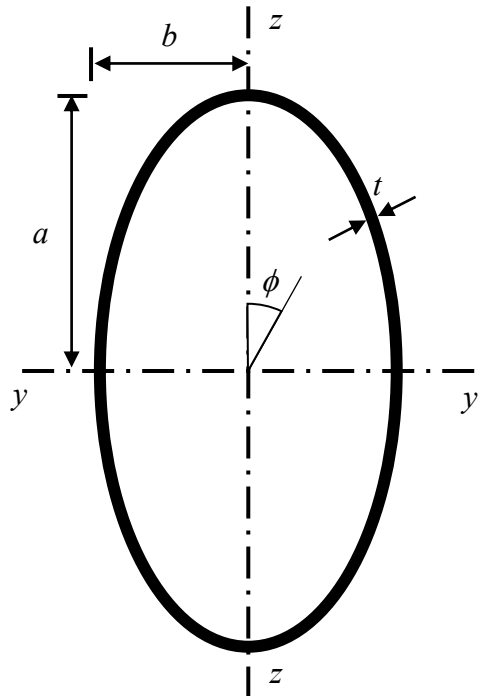

Figure 1: Cross-sectional geometry of elliptical hollow section.

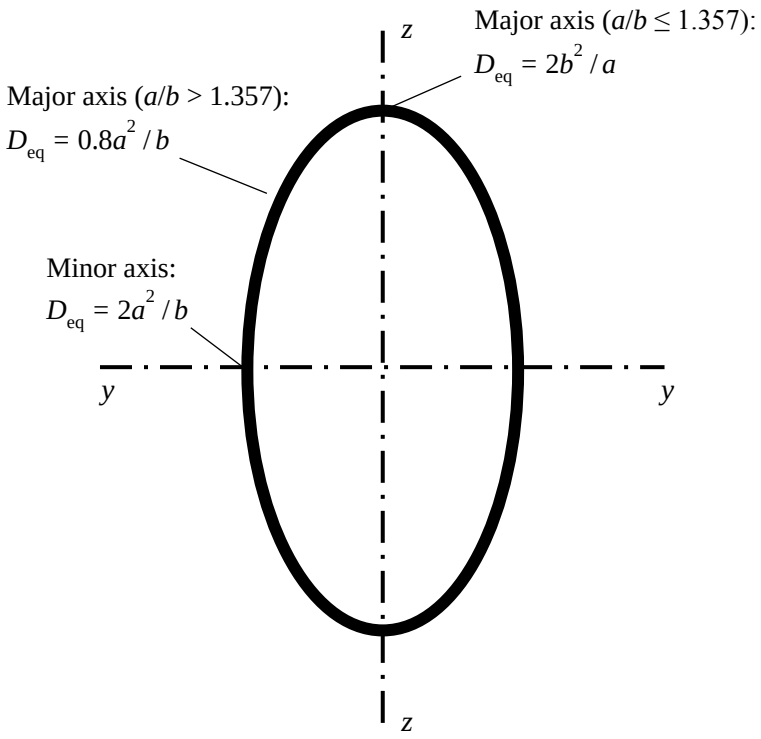

Figure 2: Location of points of initiation of local buckling and corresponding equivalent diameters.

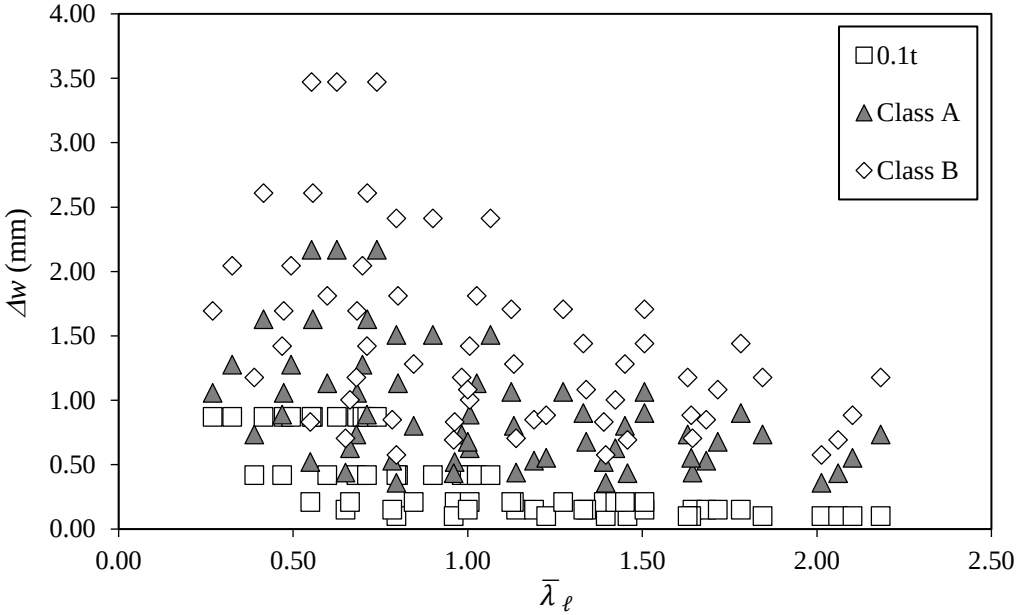

Figure 3: Imperfection amplitudes of EHS modelled in the numerical parametric study.

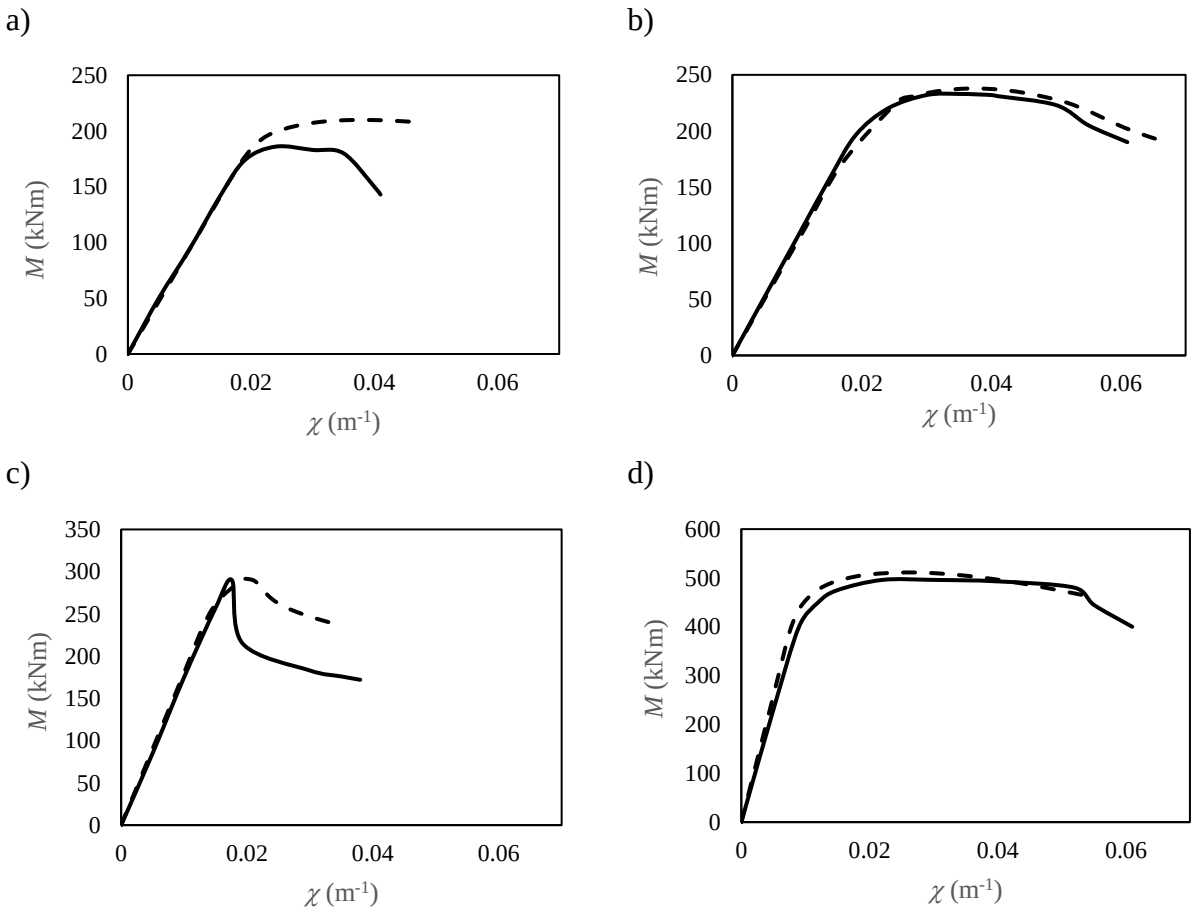

Figure 4: Comparison of experimental (solid lines) and numerical (dashed lines) moment–curvature relationships of specimens analysed in the validation study; a) 400 × 200 × 8.0 – B1 (minor axis); b) 400 × 200 × 10.0 – B1 (minor axis); c) 500 × 250 × 8.0 – B1 (minor axis); d) 500 × 250 × 8.0 – B2 (major axis).

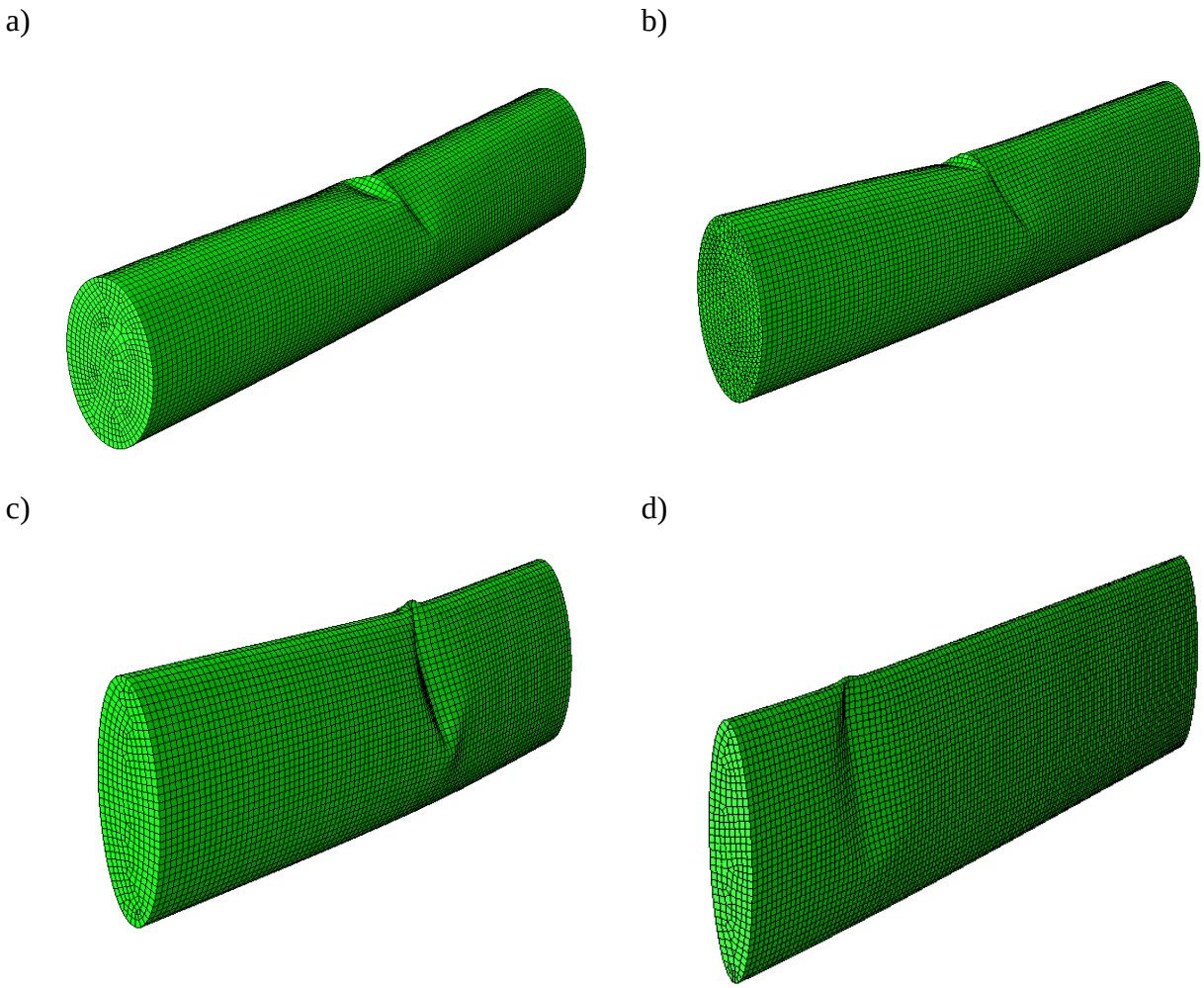

Figure 5: Typical failure modes observed in specimens bent about the major axis;
a) a/b = 1.5 (f_y = 1200 N/mm^2, t = 2.1 mm); b) a/b = 2.0 (f_y = 900 N/mm^2, t = 2.1 mm); c) a/b = 3.0 (f_y = 390 N/mm^2, t = 1.5 mm); d) a/b = 5.0 (f_y = 500 N/mm^2, t = 2.1 mm).

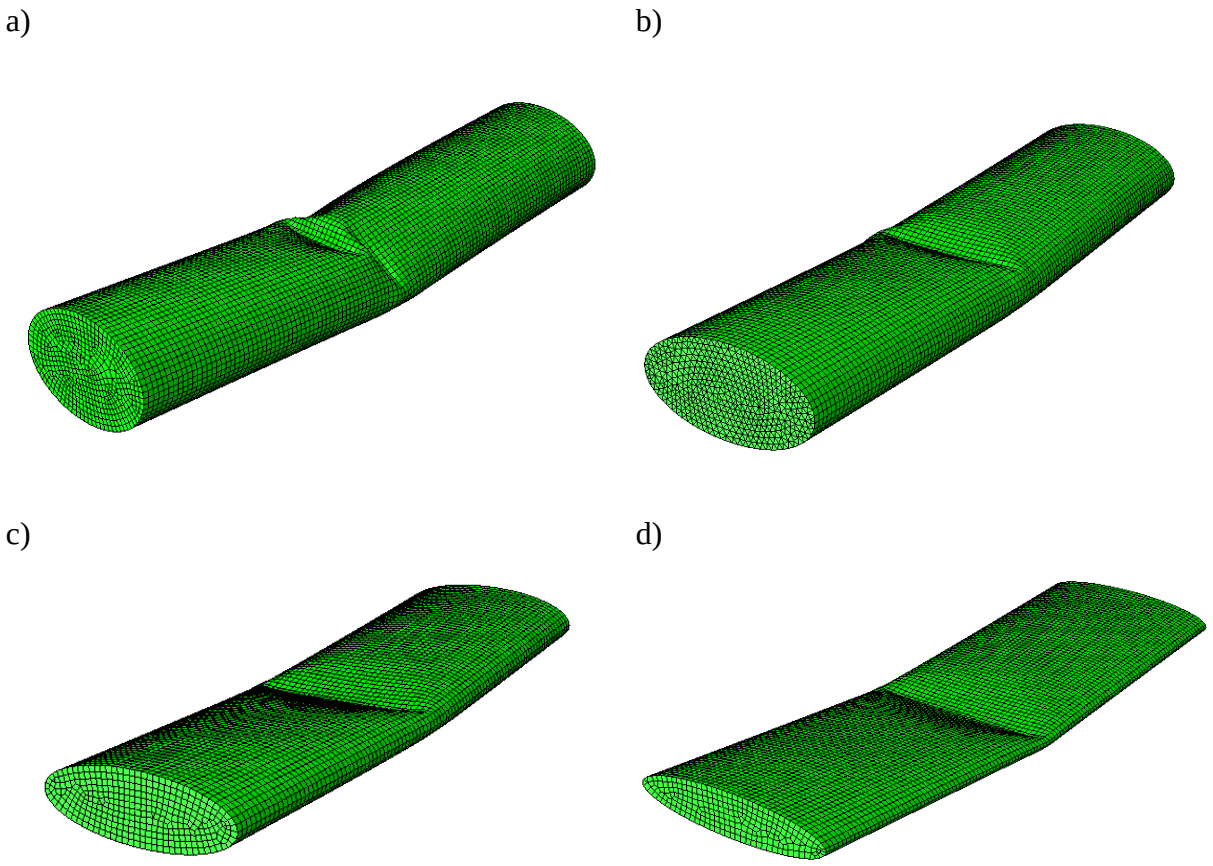

Figure 6: Typical failure modes observed in specimens bent about the minor axis;
a) a/b = 1.5 (f_y = 390 N/mm^2, t = 1.5 mm); b) a/b = 2.0 (f_y = 390 N/mm^2, t = 2.1 mm); c) a/b = 3.0 (f_y = 700 N/mm^2, t = 2.1 mm); d) a/b = 5.0 (f_y = 390 N/mm^2, t = 2.1 mm).

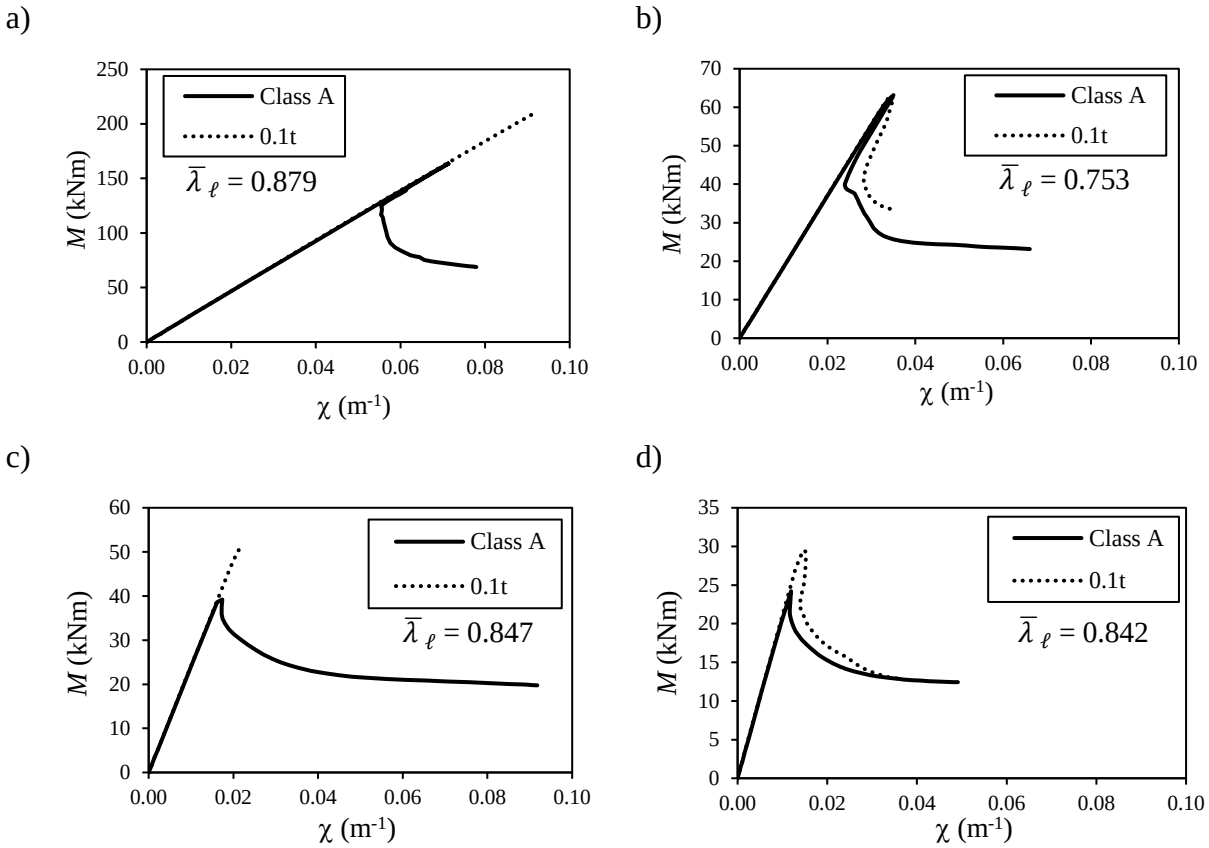

Figure 7: Typical moment–curvature responses observed in specimens bent about their major axis;
a) a/b = 1.5; b) a/b = 2.0; c) a/b = 3.0; d) a/b = 5.0.

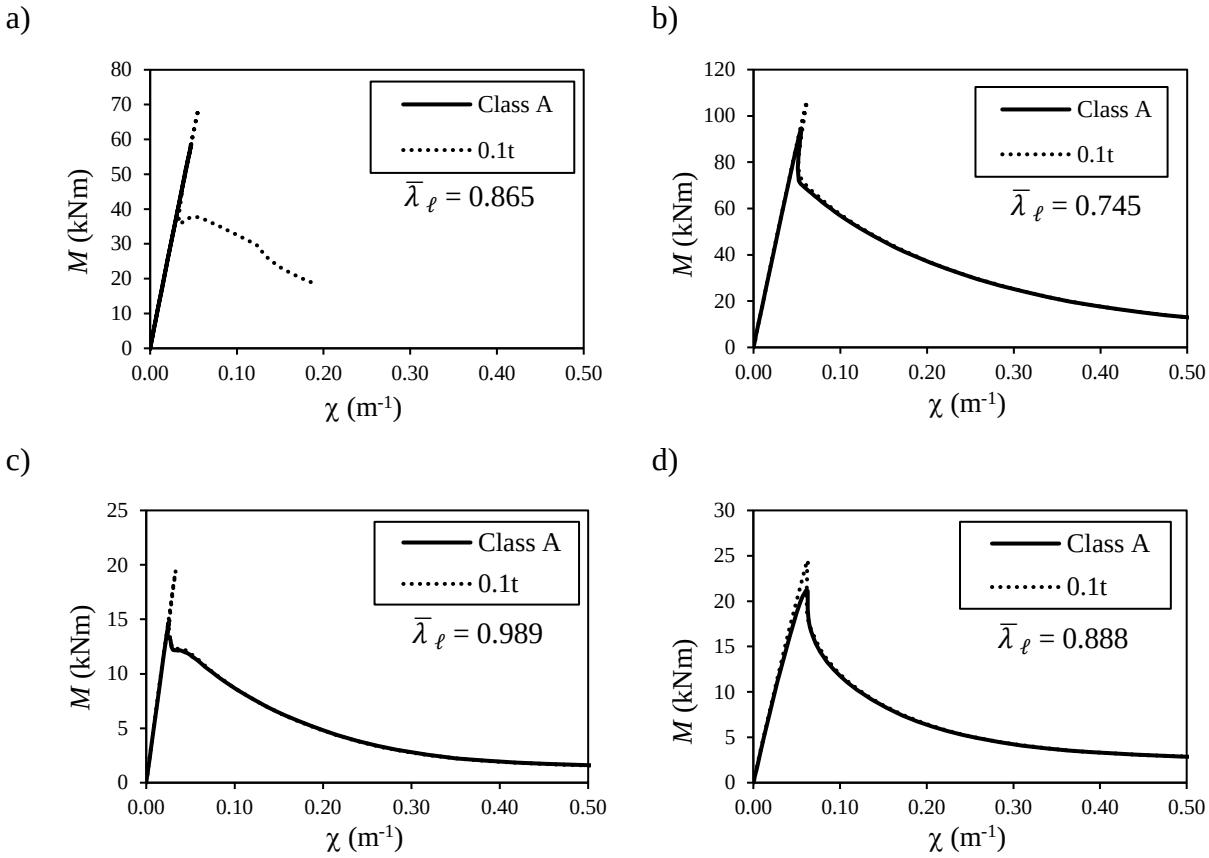

Figure 8: Typical moment–curvature responses observed in specimens bent about their minor axis;
a) a/b = 1.5; b) a/b = 2.0; c) a/b = 3.0; d) a/b = 5.0.

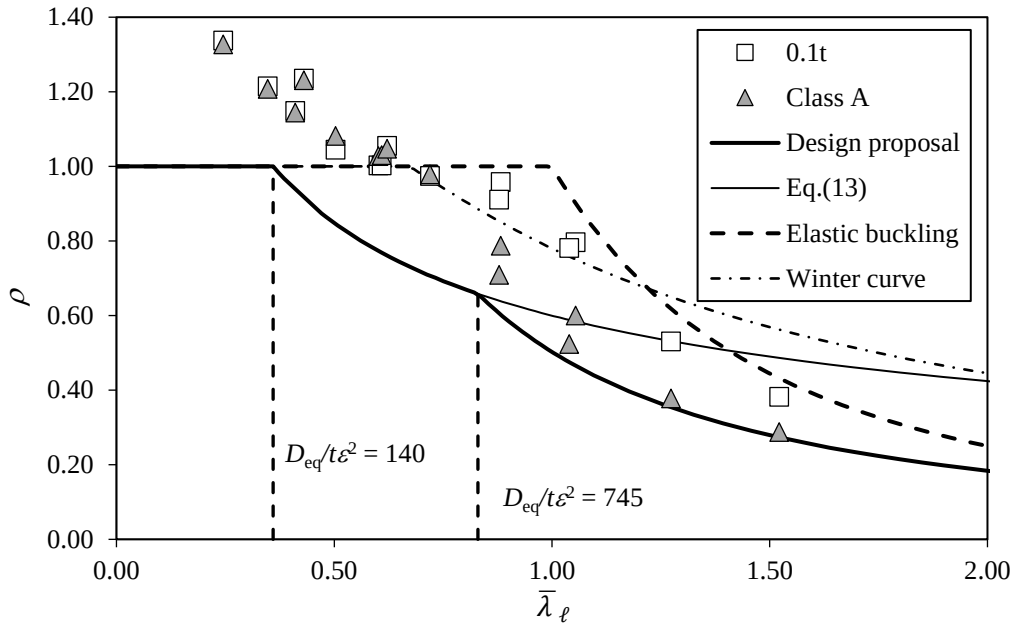

Figure 9: Local buckling reduction factors for EHS with a/b = 1.5 bent about the major axis.

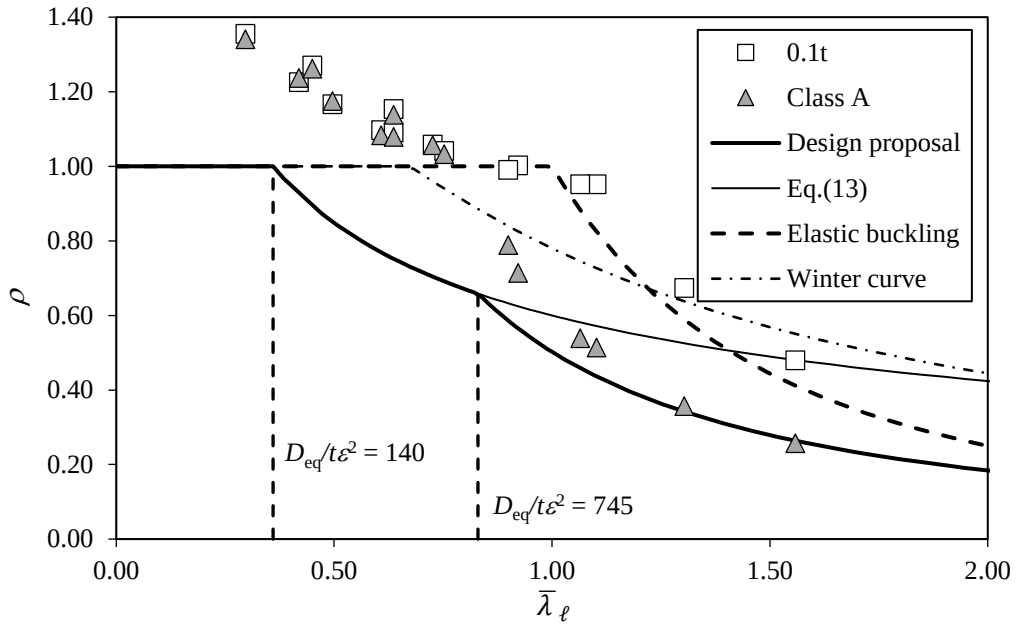

Figure 10: Local buckling reduction factors for EHS with $a/b = 2.0$ bent about the major axis.

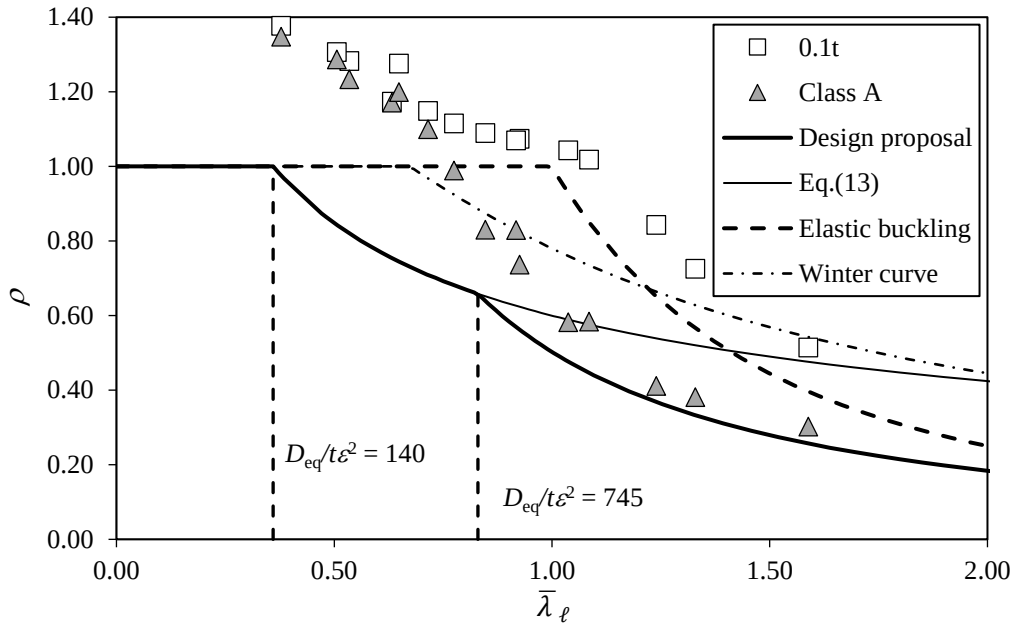

Figure 11: Local buckling reduction factors for EHS with $a/b = 3.0$ bent about the major axis.

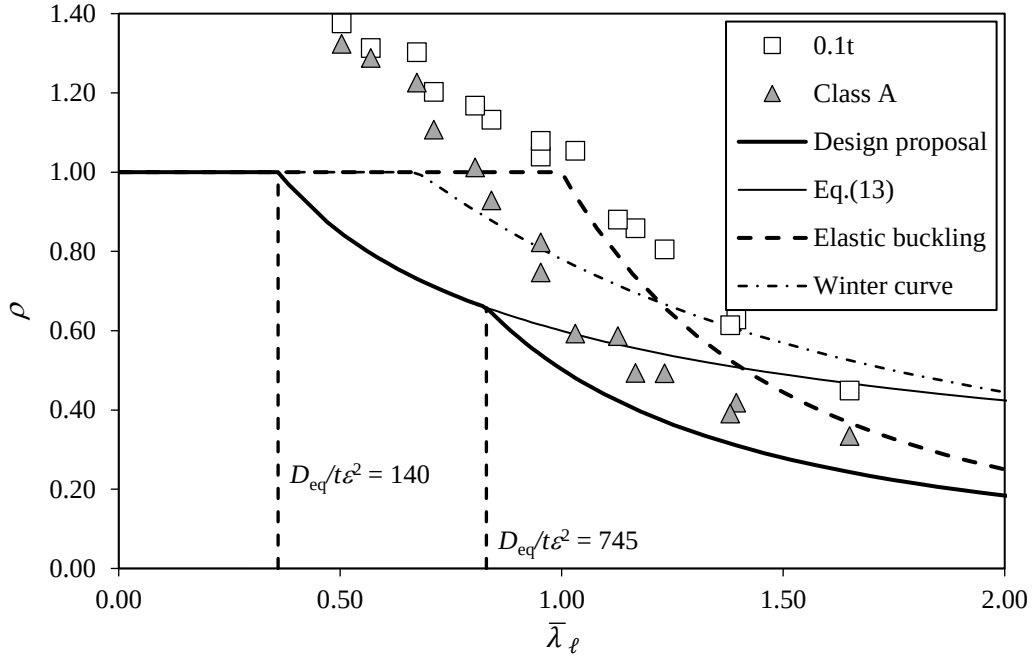

Figure 12: Local buckling reduction factors for EHS with a/b = 5.0 bent about the major axis.

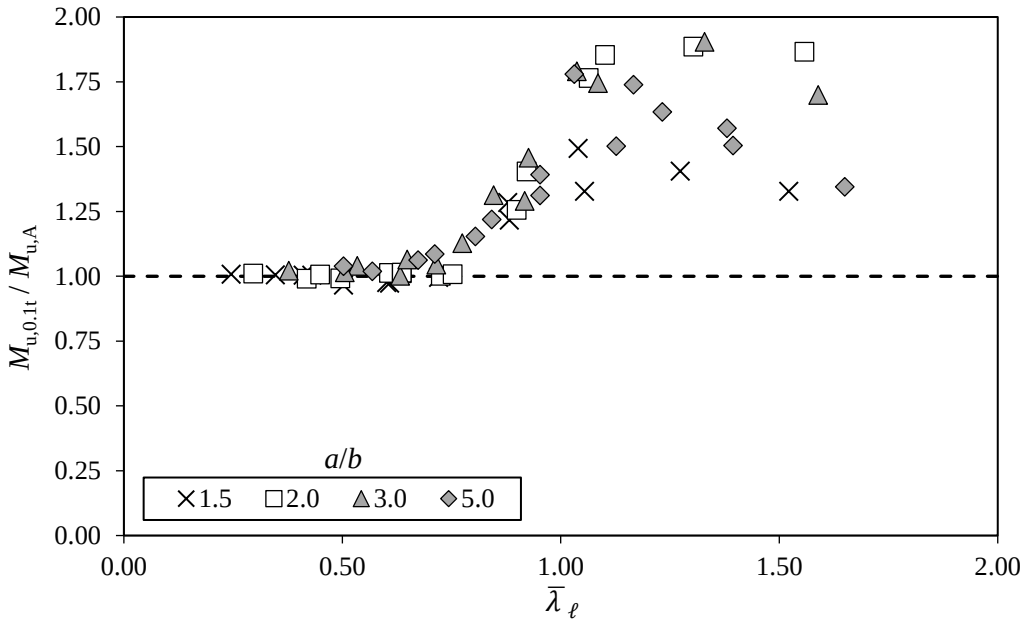

Figure 13: Imperfection sensitivity of EHS bent about the major axis for various aspect ratios *a*/*b*.

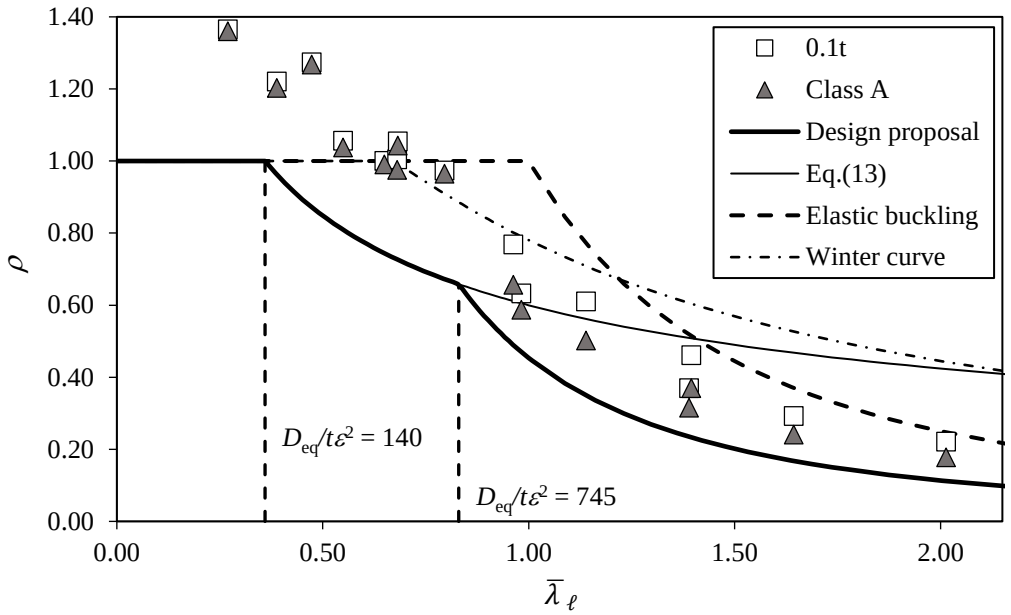

Figure 14: Local buckling reduction factors for EHS with a/b = 1.5 bent about the minor axis.

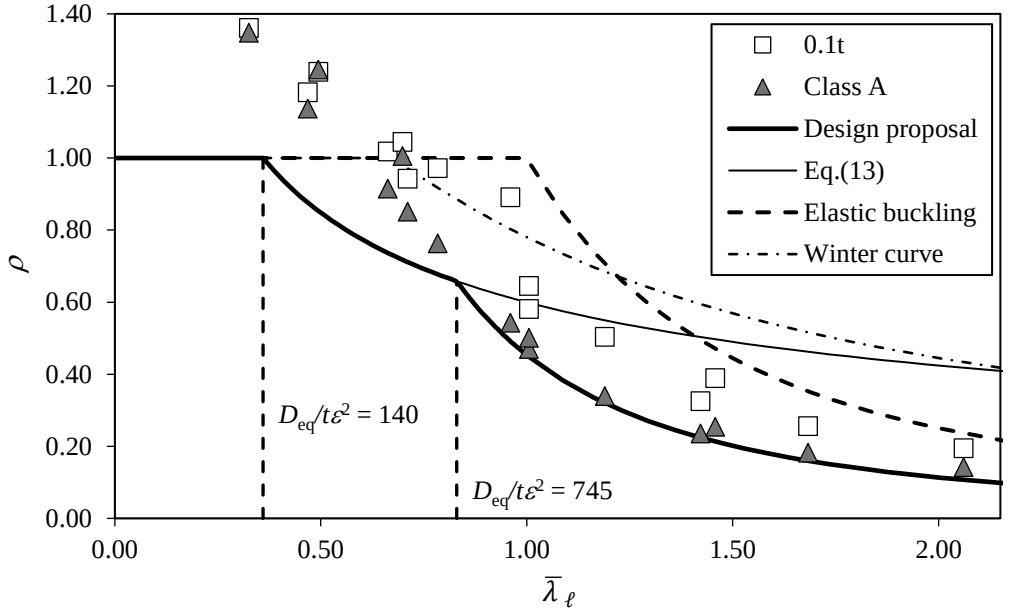

Figure 15: Local buckling reduction factors for EHS with a/b = 2.0 bent about the minor axis.

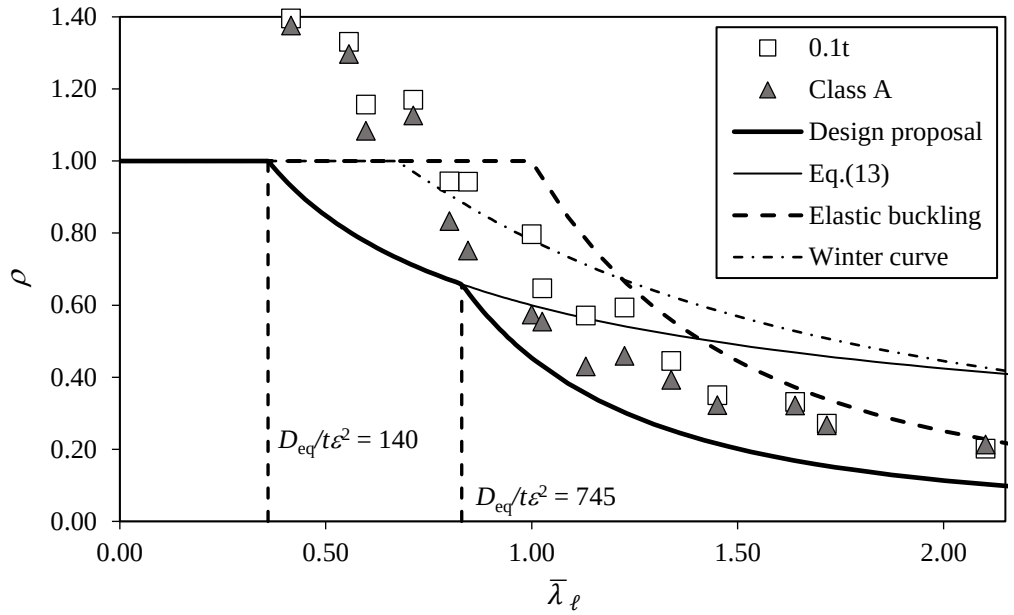

Figure 16: Local buckling reduction factors for EHS with a/b = 3.0 bent about the minor axis.

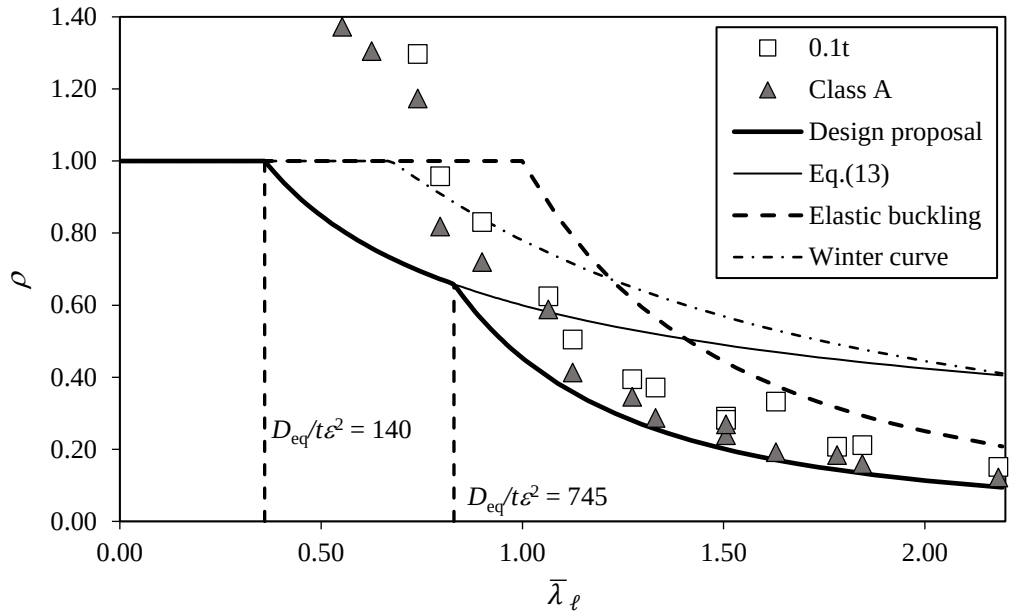

Figure 17: Local buckling reduction factors for EHS with a/b = 5.0 bent about the minor axis.

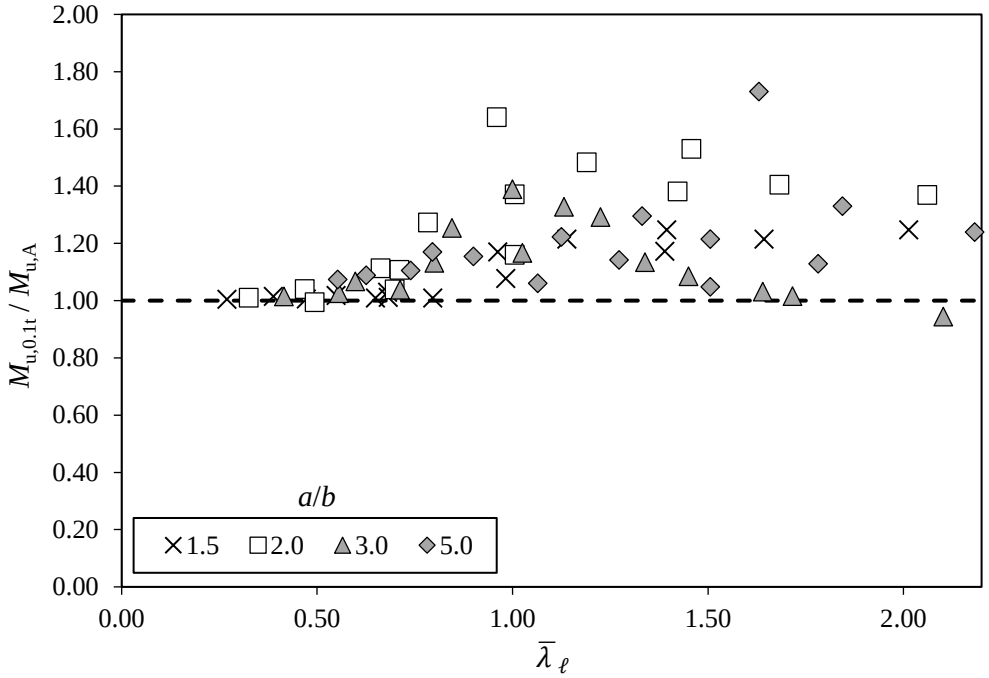

Figure 18: Imperfection sensitivity of EHS bent about the minor axis for various aspect ratios *a*/*b*.

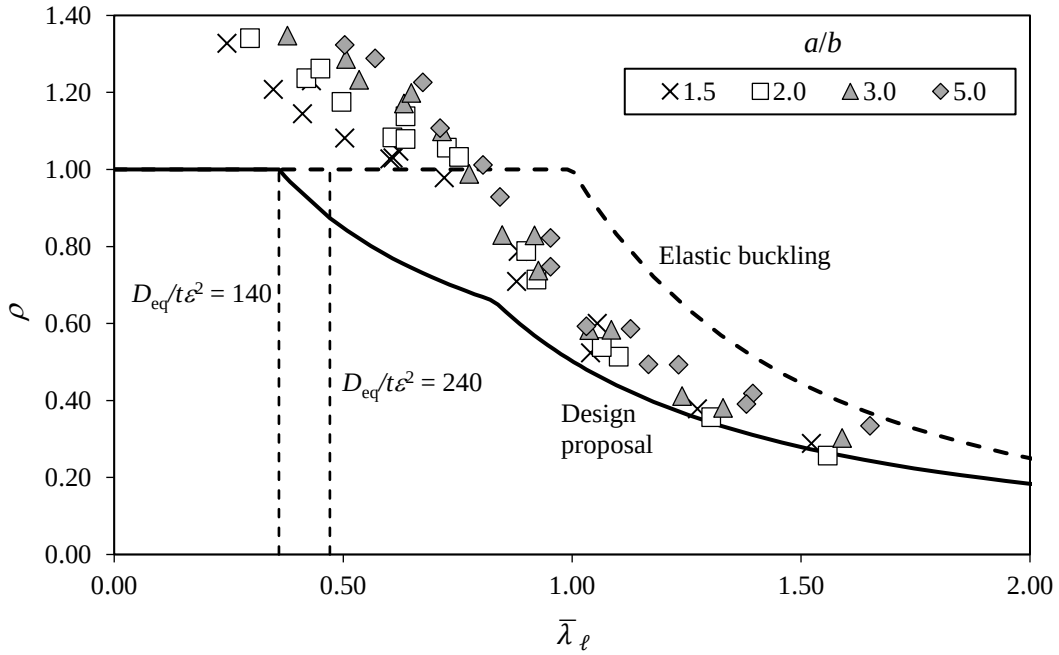

Figure 19: Proposed design curve for slender EHS bent about the major axis.

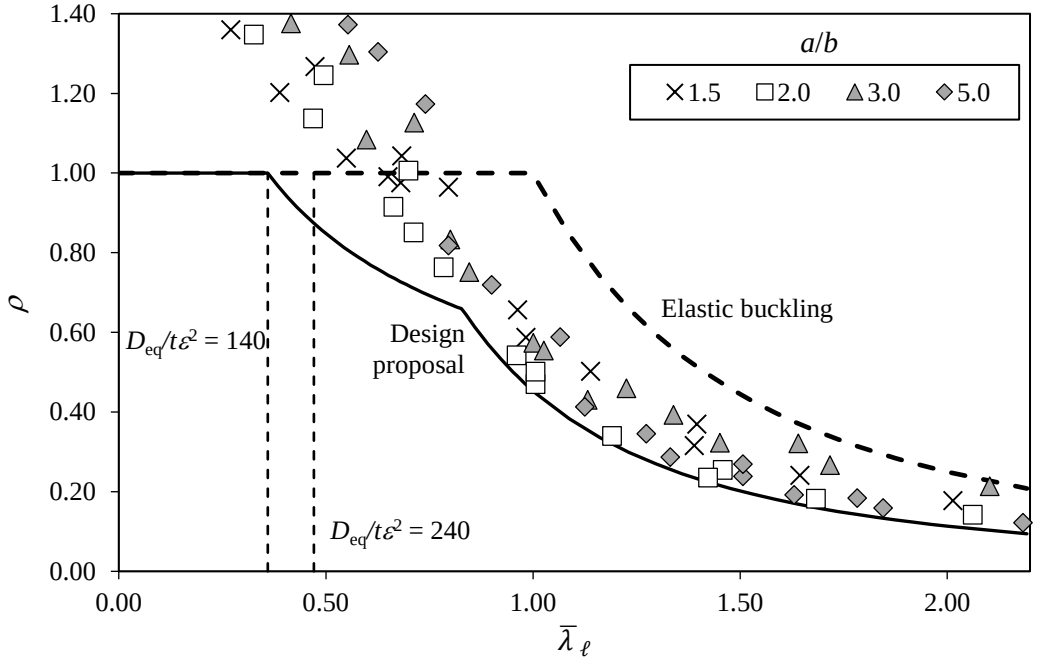

Figure 20: Proposed design curve for slender EHS bent about the minor axis.

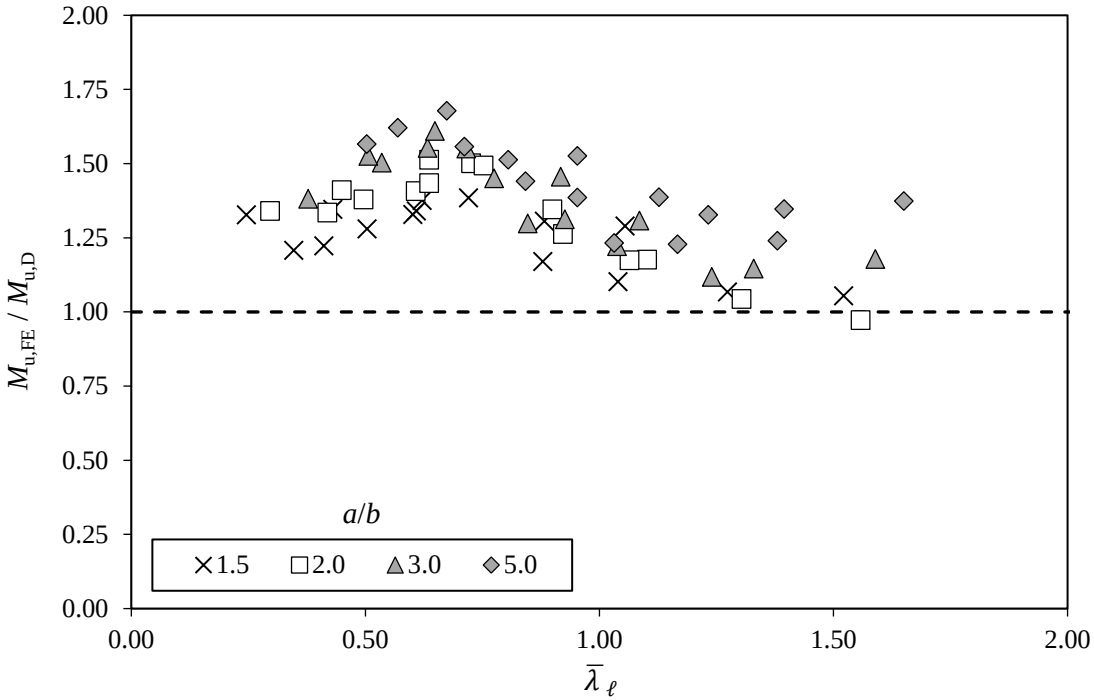

Figure 21: Ratios of numerical ultimate moment to design ultimate moment for EHS bent about the major axis for various aspect ratios *a*/*b*.

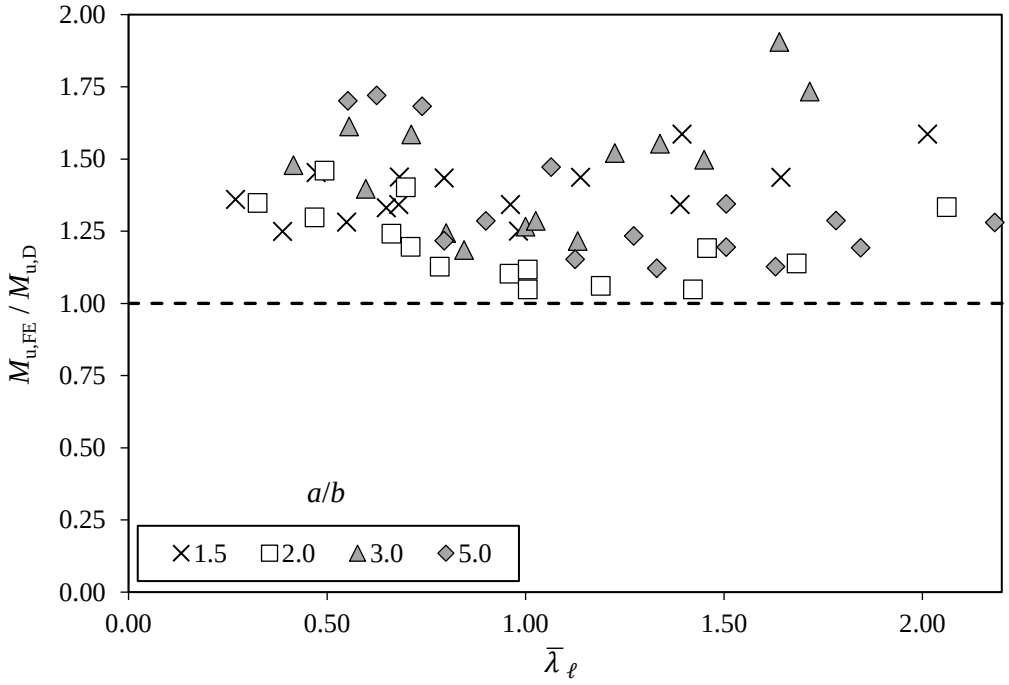

Figure 22: Ratios of numerical ultimate moment to design ultimate moment for EHS bent about the minor axis for various aspect ratios *a*/*b*.